

RADIATION RESISTANT SUPERFERRIC MAGNETS FOR FRAGMENT
SEPARATORS

By

Jonathan David DeLauter

A THESIS

Submitted to
Michigan State University
in partial fulfillment of the requirements
for the degree of

MASTER OF SCIENCE

Department of Physics and Astronomy

2006

ABSTRACT

RADIATION RESISTANT SUPERFERRIC MAGNETS FOR FRAGMENT SEPARATORS

By

Jonathan David DeLauter

Several proposed accelerator facilities will be capable of providing intense beams on targets that are in close proximity to superconducting magnets. These magnets will have to operate in high-radiation environments. This work examines a metal-oxide insulated version of the standard CICC (Cable-in-Conduit Conductor) as a proposed solution for radiation levels directly following the target, and examines a cyanate-ester as a proposed solution for lower radiation areas in the separator. A small superferric dipole, similar to one previously constructed with conventional epoxy-potted coils, has been fabricated with metal-oxide CICC and, separately, with cyanate ester. Both technologies have been tested and results are reported.

Copyright by
JONATHAN DAVID DELAUTER
2006

ACKNOWLEDGEMENTS

The author would like to thank A. Zeller for advice, instruction, help, patience, providing unlimited opportunity and helping me follow it through; J. C. DeKamp for instruction, patience, and for sharing his skills and experience; Chen-yu Gung and others at MIT Plasma Science and Fusion Center for sharing their magnet facility and their help; B. Sherrill and F. Marti for volunteering their time on my committee; D. Pendell for welding help and expertise; J. Bierwagen, S. Bricker, and J. Gonzales for project advice; J. Savory and D. Arthur Brown for labor and project advice; T. Hudson and others at BPS Machine Shop for machining instruction and advice. Thanks to Mom, Dad, and Mike for their support.

TABLE OF CONTENTS

LIST OF TABLES	vi
LIST OF FIGURES	vii
1 INTRODUCTION	1
1.1 Radiation	2
1.2 Cyanate-ester.....	4
1.3 Metal-Oxide Insulated Cable-in-Conduit Conductor (MOCICC)	6
2 THE CYANATE-ESTER DIPOLE.....	10
2.1 Design of the Cyanate-ester Dipole	10
2.2 Construction of the Cyanate-ester Dipole.....	17
2.3 Testing of the Cyanate-ester Dipole	21
2.4 Simulation of Quench in the Cyanate-ester Dipole	23
2.5 Discussion of the Cyanate-ester Dipole.....	28
3 THE METAL OXIDE CICC DIPOLE.....	30
3.1 Design of the MOCICC Dipole	30
3.2 Constructing the metal-oxide CICC dipole magnet.....	41
3.3 NSCL Test Results.....	48
3.4 October 2006 MIT Test Results.....	50
3.5 Analysis:	58
3.6 Further Research	60
4 CONCLUSIONS.....	62
5 APPENDICES	63
5.1 Cyanate-Ester Winding Instructions.....	63
5.2 Cyanate-Ester Winding Photo Flow-Chart	65
5.3 Gandalf Input File for MOCICC Dipole; Operation in 4 W/m Heating.....	66
6 BIBLIOGRAPHY.....	67

LIST OF TABLES

Table 2-1: Wire, coil, and magnet parameters for the cyanate-ester dipole.	12
Table 2-2: Problems encountered during the winding of the cyanate-ester coils.....	19
Table 3-1: Magnet and Wire Parameters for the MOCICC Dipole	38

LIST OF FIGURES

Fig. 1-1: Diagram of a fragment separator. The fragment separator is composed mainly of dipole and quadrupole magnets. In high radiation conditions the magnets that succeed the target have the most exposure. Radiation levels drop significantly further down the beamline in the separator due to the energy lost in beam dumps through the dipole magnets. 8

Fig. 1-2: Metal oxide insulated cable-in-conduit conductor. The outer and inner conduits are 316 stainless steel, about 1 mm thick each. The white layer is MgO and is about 2 mm thick. The entire cross section is 1 cm x 1 cm. The inner conduit contains strands of copper/NbTi. 9

Fig. 2-1: This shows the QUENCH [Ref. 12] simulation of the quench voltages (for various currents) in the coil during a quench. The insulation around the wire was rated for 689 V (between two strands). These results demonstrate that the operating current used, which was near 54 A, would not damage the coil through arcing if a quench were to occur. 13

Fig. 2-2: Examples of a Stycast® epoxy-potted coil (in back) and a CTD-422 cyanate-ester-potted coil (in front). 14

Fig. 2-3: The field lines calculated with POISSON [Ref. 13] for one symmetric quarter of the cyanate-ester dipole. The units for the x and y axis are cm. 15

Fig. 2-4: The short sample current limit guaranteed by the manufacturer (Supercon, Shrewsbury, MA) is plotted along with the field (at the conductor) and required current calculated by POISSON [Ref. 13]. Their intersection, about 50 amps, is the estimated short sample current of the magnet [Ref. 4]. 16

Fig. 2-5: The complete magnet assembly hangs from the Dewar lid ready to be tested. Visible are the lead connections to the Dewar leads, magnet iron, coils, G-10 spacers, and voltage taps. Partially visible are the coils shims, solder-connected leads, and solder-connected lead fixture. 20

Fig. 2-6: Shown here is the ratio of applied current to short sample current (50 A) at the time of quenching [Ref. 4]. 22

Fig. 2-7: The current measured in the cyanate-ester dipole during a quench, matched to simulation data from the code QUENCH [Ref. 12]. The best fits were for a transverse heat propagation velocity ratio of around 1.4 % ($g=0.014$). Inductively coupling the iron (denoted as ‘with iron’ above) in the simulation did not significantly vary the result. Simulations fit to Stycast®-potted coils have a transverse heat propagation velocity of about 7%. 24

Fig. 2-8: The voltage measured in the cyanate-ester dipole during a quench, matched to simulation data from the code QUENCH [Ref. 12]. The best fits were for a transverse heat propagation velocity ratio of around 1.4 % ($g=0.014$). Inductively coupling the iron (denoted as ‘with iron’ above) in the simulation did not significantly vary the result. Voltages during the quench did not approach levels that would damage the coils..... 25

Fig. 2-9: The first derivative was calculated for the measured current and for the QUENCH-simulated current [Ref. 12]. The first derivative of current corresponds well to the voltage measurements. 26

Fig. 2-10: The second derivative of current with respect to time for the quench data measured, and for two simulations from QUENCH [Ref. 12]. Inductively coupling the iron (denoted ‘with iron’) in the QUENCH [Ref. 12] input did not significantly vary the result..... 27

Fig. 3-1 continued: GANDALF-simulated [Ref. 18] time evolution and equilibrium of pressure, massflow, and temperature. A 4 W/m (representative of the 150 W into the first RIA quadrupole) radiation-heat load was used. The reason for the drop-off at $x=3.6$ is because the conduit ends there; the liquid helium is exiting the conduit. I) Liquid helium flow pressure reaches equilibrium around 4.6 atm (at a distance of $x=1.8$ m down the length of the conduit). II) Liquid helium mass flow reaches equilibrium at 4.87 kg/s (at a distance of $x=1.8$ m down the length of the conduit). III) Conductor temperature along the length of the conduit at times 0.1 s (A), 1.0 s (B), 4.0 s (C). The temperature profile does not change after $t=4.0$ s; curve c represents the equilibrium temperature profile along the conduit. 35

Fig. 3-2 continued: GANDALF [Ref. 18] simulation of the propagation of a quench. The quench was induced by a 400 W/m, 0.01 s heat pulse distributed from $x=1.7$ m to $x=1.8$ m in the center of the 3.6 m conduit of the MOCICC dipole. The conduit has a helium flow of 5 g/s at 5 atm. The quench lasts only 0.01 s, so the time on the graph essentially represents the time following the quench. I) The power-supply current was deactivated along an exponential decay, with time constant 0.1 s. II) Voltage between the conductor and ground (the outer stainless steel jacket) peaks at about 1 V in this quench; there is only about 2 kJ of stored energy in the magnet. III) The temperature at 0.01s (the end of the heat pulse) was not dangerous to the magnet..... 37

Fig. 3-3: The short-sample current limit (for the individual wire strand) is represented by the intersection (about 290 A at about 2.5 T maximum field on conductor) of the circle points, POISSON-simulated [Ref. 13] fields for given currents, and the diamond points, the critical current of the amount of NbTi material that is in the wire used (NbTi data from an Otokompu table of NbTi material properties). Also shown are the guaranteed, typical, and actual current-field specs provided by the manufacturer, Supercon. 39

Fig. 3-4: The magnetic field lines for the top-right quarter (symmetry) of the MOCICC dipole cross-section, calculated by POISSON [Ref. 13], for 40 kA•turns. The x and y axes represent the x and y directions and the units are cm.	40
Fig. 3-5: A steel winding arm pivots inside the winding-form cylinders to wind the coil into shape. The cylinders have a 2" outer diameter and are welded onto the plate beneath them. During winding, tack welds were placed occasionally to maintain the shape.	44
Fig. 3-6: The MOCICC dipole hangs from the NSCL Dewar lid, ready to be tested. On the left is the lead connection between the two coils.....	45
Fig. 3-7: The joint that connects the coils in series is comprised of the solder wire bundle surrounded by two clamshell halves made of an outer stainless steel jacket with a Macor® insert to prevent the conductor from making contact with ground. Seen here is a cutaway: one of the two clamshell halves.	46
Fig. 3-8: The completed lead connection joint is seen here, secured to the magnet iron by a post. The two clamshell halves were welded in place around the soldered bundle.	47
Fig. 3-9: The MOCICC dipole hangs under the NSCL dunking Dewar lid, ready to be tested. The magnet leads have been connected to the Dewar leads.....	49
Fig. 3-10: MOCICC dipole magnet ready to be inserted into MIT's Dewar. The large Dewar leads are helium gas cooled.....	52
Fig. 3-11: Close-up view of the lead connections. The short magnet lead on the right is connected to the Dewar lead by some clamped Rutherford superconducting cable, which quenched during the testing. Labels have been applied that correspond to the diagram in Fig. 3-12.....	53
Fig. 3-12: Diagram of the test instrumentation inside the Dewar. V_1a and V_1e are voltage taps on the left and right (respectively) connections between the Dewar leads and the magnet leads. V_1c and V_1d are voltage taps a nearly-co-wound coil for measuring induced voltage. V_1b is a voltage tap to measure the magnet voltage. The liquid helium level sensor instrumentation is labeled V_2a through V_2d. On the right hand side of the diagram are the liquid helium levels needed to reach the specified heights in the Dewar; a height between 40% and 50% was desired.....	54
Fig. 3-13: The instrumentation setup at MIT. Data were recorded by a Macintosh computer (bottom left), a Yukagawa LR8100 8-channel data recorder (top), and three digital voltmeters (top-left).....	55
Fig. 3-14: Measurements during the ramp-up of the magnet (ramp #5 according to Fig. 3-15) from the voltage taps V1_a and V1_e (labeled according to Fig. 3-12), the	

bridge connections between the coil leads and the Dewar leads.). V1_e begins to generate resistive voltage shortly before the quench (the quench occurred after 3.5 s) and V1_a is very noisy during the entire ramp. The magnitude of the noise on V1_a is much higher than the resistive voltage on V1_e. It is likely that the noise on V1_a was generated by wire movement, and was the cause of the premature quench of the magnet. The ramp rate for this test was 700 A/s. The other tests, at various ramp rates, showed similar results. 56

Fig. 3-15: Quench history of the MOCICC dipole test at MIT. The magnet could not be ramped to its full sustainable current due to problems with the connection between the Dewar leads and the magnet. By increasing the ramp rate, the magnet current could be pushed farther before heat propagating from the quench in the lead connection would initiate a quench in the magnet. Error in the measurement due to sampling rate is shown with thick, solid error bars. For the last four measurements, the measurement was read from voltmeters, which did not agree with the measurement read by the computer. This discrepancy is represented by light, dotted error bars. 57

1 INTRODUCTION

High intensity accelerators like GSI (Gesellschaft für Schwerionen-forschung, Darmstadt, Germany) [Ref. 1], and the proposed Isotope Science Facility (ISF), a revision of the Rare Isotope Accelerator (RIA) [Ref. 2], require superconducting magnets to operate in high radiation environments. The radiation leads to problems with neutron heating and long-term radiation damage, which existing superconducting magnet designs cannot address. A high radiation environment is the target-in area in front of the fragment separator, which consists mainly of dipole, quadrupole, and sextupole magnets (Fig. 1-1). The magnets function to bend and focus the trajectory of the beam. Fragment separator magnets are superferric (iron-dominated and superconducting) due to needs for high magnetic field magnitude, uniformity, and aperture. This work examines cyanate-ester and metal-oxide insulated cable in conduit conductor (CICC) technologies as solutions for developing radiation tolerant (radiation resistant) magnets.

1.1 Radiation

The radiation problem can be divided into nuclear heating and long-term radiation damage. Radiation exiting the target can be composed of ions, neutrons, electrons, muons, and gamma rays. Magnet coils can be shielded from gamma rays and ions, but shielding is not effective for neutrons. The flux of neutrons dissipates energy in the form of heat into the material. The energy and heat distributed depends on the energy of the neutrons and the mass of the material. For this reason the cold mass, the mass of material that is being cooled by the liquid helium, must be kept as small as possible.

The first quadrupole coil in the triplet that follows the target in the RIA fragment separator has a calculated dose rate, for some combination of beam and target, of 1 Gy/s from a 400 kW heavy ion beam [Ref. 3]. With an assumed operation time per year of 10^7 s (about 3000 hr), there is a yearly dose of 10^7 Gy (10 MGy). A sextupole magnet precedes the first quadrupole triplet, and another triplet follows (Fig. 1-1), all of these will be subject to similarly high radiation levels and need an inorganic radiation resistant technology [Ref. 4]. Beyond these magnets and after the beam dump in the first dipole, the beam power drops to at most 10 kW. It is in this area that the cyanate-ester would be applicable. 10 kW is only a fraction of the original 400 kW beam, but organic materials have a factor of 200 more radiation sensitivity than inorganic [Ref. 5]. Thus, the organic radiation dose expected in these areas is at most 5 MGy, making it suitable for the cyanate-ester material.

GSI has a similar configuration, with the expected dosage in the first coil of 14 MGy/yr, or a total dose of 280 MGy [Ref. 6]. The later magnets in the GSI fragment

separator, for reasons comparable to RIA, are likely to have radiation levels low enough for the use of cyanate-ester.

Over a long period of time (one to many years), depending on material and exposure rate, radiation can damage coil materials. Organic materials are especially sensitive to this radiation because they are composed of molecular chains, which have low binding energies (compared to a metal lattice for example) and can be split easily by radiation [Ref. 7]. Hydrogen bonds are especially sensitive to this type of radiation and cyanate esters generally have about half as many hydrogen bonds as normal epoxies. Damage due to radiation can radically change the physical properties of these materials, and in practice leads to irreparable weaknesses. Strong Lorentz forces can exacerbate these weaknesses, and shorting or quenching of a coil can occur through failure of the epoxy or electrical insulation.

1.2 Cyanate-ester

The majority of the beam energy is dumped into the first few magnets in the fragment separator, and past these magnets the radiation levels are much lower, although still hazardous to epoxies normally used for magnets. In these areas a radiation resistant organic compound called cyanate-ester may be suitable [Ref. 5]. The cyanate-ester has radiation tolerance much greater than standard epoxy, with equivalent compression strength, but lower shear strength [Ref. 8]. It was proposed as the solution for the lesser radiation areas at GSI and RIA. A cyanate-ester, CTD-422, formulated by CTD (Composite Technology Development, Lafayette, CO), for use in fusion research, was used to wind a radiation resistant dipole for the purpose of researching the use of cyanate-ester for coil winding.

CTD's 400 series cyanate-ester has been irradiated and compared with standard epoxies [Ref. 8]. It was found that the compressive strength of epoxies starts to break down above 2.0×10^{22} neutrons \cdot m⁻², whereas the compressive strength of the cyanate-esters tested did not show significant degradation up to 5.0×10^{23} neutrons \cdot m⁻². The cyanate-ester's shear strength is comparable to epoxy and degrades similarly in radiation. Thus, cyanate-ester can be used as a more radiation-resistant substitute for epoxy in designs that reduce shear and keep the insulation in compression [Ref. 7].

Factors especially important to consider in the design of an epoxy or cyanate-ester magnet are the stored energy, transverse heat propagation velocity, thermal conductivity, quench voltages and other factors that affect quenching. For the cyanate-ester magnet, the radiation tolerance of the materials was an important consideration.

A small superconducting magnet must be capable of releasing its stored energy before the coil voltage rises to a dangerous point where it can arc between turns, shorting and destroying the coil. The transverse heat propagation velocity is important because it is the primary factor in how quickly a local quench will spread through the coil. When a local quench occurs it is important to quench the rest of the coil as quickly as possible so that high voltages do not build up at the local quench location.

1.3 Metal-Oxide Insulated Cable-in-Conduit Conductor (MOCICC)

The proposed technology uses cable in conduit conductor (CICC) technology with a metal-oxide ceramic as an interturn insulator, an example of which can be found in Fig. 1-2. Metal-oxide-insulated CICC (MOCICC) have the advantage that all of the materials used (see material radiation tolerance table) have radiation tolerances greater than or equal to that of the superconductor (about $5 \cdot 10^8$ Gy). These coils are expected to operate in the high radiation environments of the fragment separator.

There are few technologies with radiation tolerance on the order of 10^8 Gy, and of them only the resistive mineral-insulated-conduit (MIC) is scalable. Research done on internally anodized aluminum MOCICC found that current densities of up to 70 A/mm^2 were achieved and it was estimated that current densities of up to 100 A/mm^2 were possible with more R&D [Ref. 5]. However, those coils were small and no way has been found to scale the technology to larger magnets. The first quadrupole in the separator receives radiation as high as 2 Gy per second [Ref. 5].

Resistive mineral-insulated-conduit (MIC) magnets are well established and have been used in PSI and LANL [Ref. 9, Ref. 10]. This technology has been used for 30 years, but has low current densities on the order of 2 A/mm^2 . The low current densities make the resistive version of this technology suitable only for where high current density is not required, like dipole magnets [Ref. 3]. Quadrupole magnets, which need high current density, will require a different technology. Superconducting MOCICC has current densities of 43 A/mm^2 established, and about 100 A/mm^2 expected. This is one to two orders of magnitude better current density than the MIC, with similar radiation tolerance.

Metal oxide CICC allows forced-flow of liquid helium through and among the conductor strands, which results in excellent conductive and convective cooling and heat removal. In addition, MOCICC is easy to incorporate in a warm-iron design because it does not need an external helium vessel. A warm-iron design cryogenically/thermally separates the coil mass from the cold mass such that the liquid helium only cools the coil mass. The warm-iron design is optimal because the iron absorbs 10 kW of radiation heat regardless of the temperature; trying to remove this much heat at 4K is prohibitively expensive.

This MOCICC technology is scalable, the insulation and stainless steel inner and outer jackets occupy a large fraction of the CICC cross section in this work, leaving only a small fraction for the conductor, but higher current densities can be achieved by increasing the size of the overall cross section without increasing the thickness of the steel or MgO layers. This would provide a higher ratio of conductor to cross sectional area, but it would increase the operating current as well. Higher operating current requires more refrigeration; i.e. 10 kA current leads require 30 L/hr of liquid helium, 50 kA leads require 150 L/hr of liquid helium, and these heat loads would be present even when the beam was off [Ref. 11]. An operating current limit of 10 kA was preferred for this work, so the cross section was limited to about 10 mm x 10 mm.

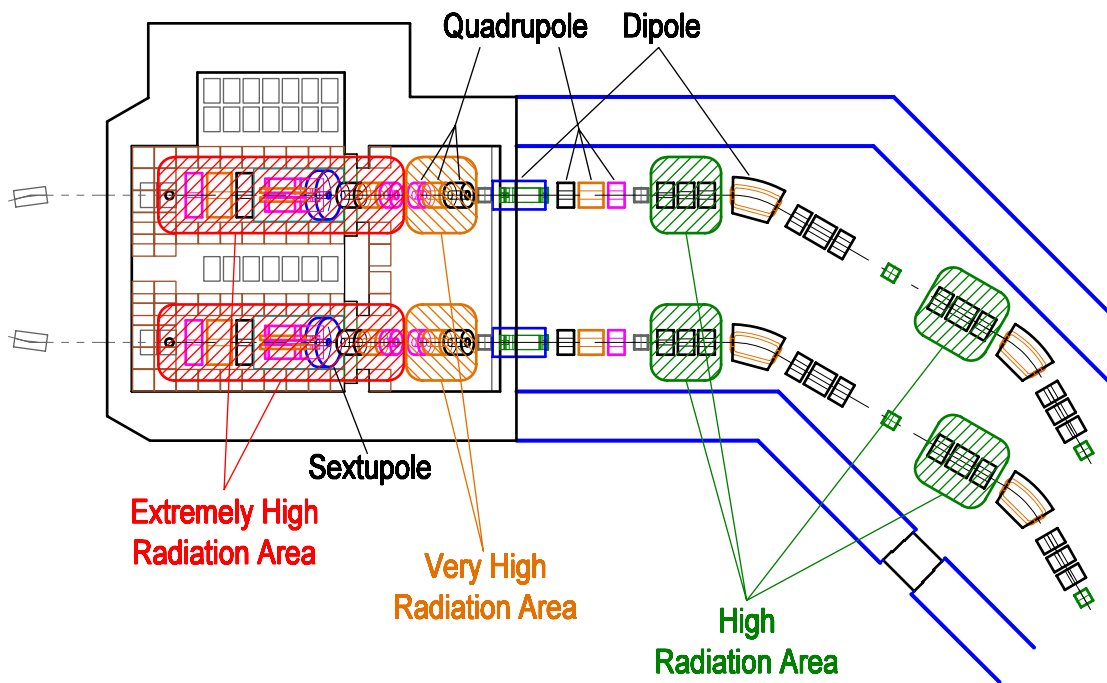


Fig. 1-1: Diagram of a fragment separator. The fragment separator is composed mainly of dipole and quadrupole magnets. In high radiation conditions the magnets that succeed the target have the most exposure. Radiation levels drop significantly further down the beamline in the separator due to the energy lost in beam dumps through the dipole magnets.

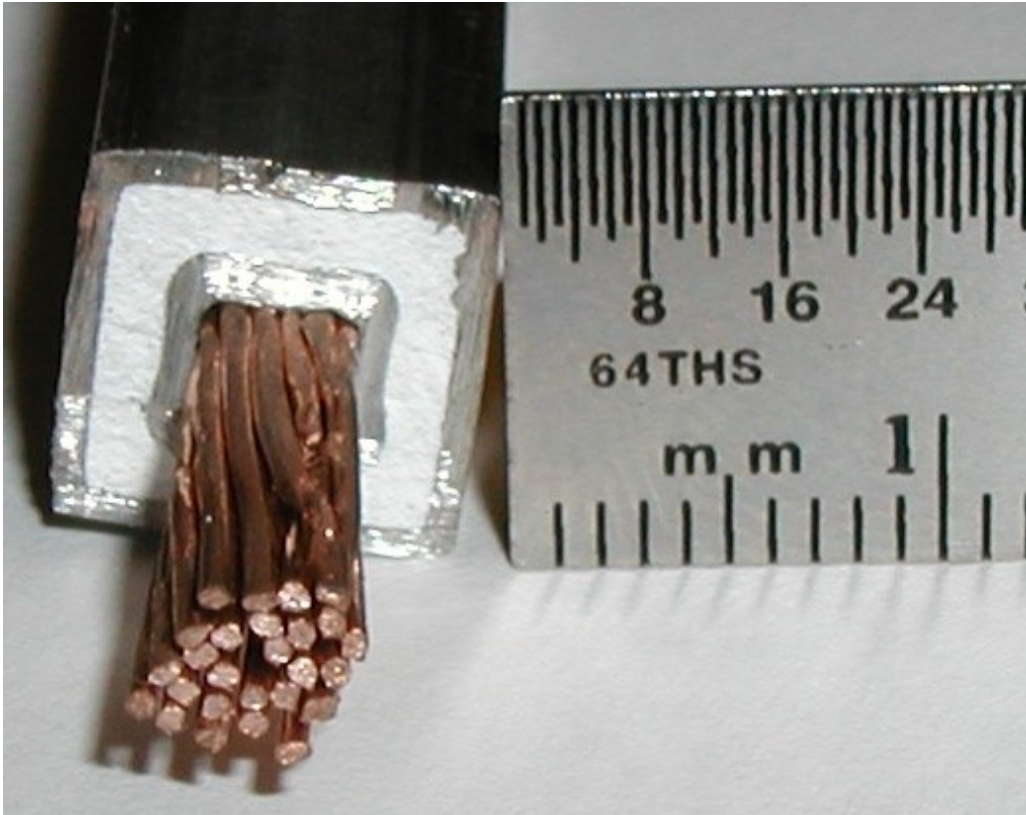


Fig. 1-2: Metal oxide insulated cable-in-conduit conductor. The outer and inner conduits are 316 stainless steel, about 1 mm thick each. The white layer is MgO and is about 2 mm thick. The entire cross section is 1 cm x 1 cm. The inner conduit contains strands of copper/NbTi.

2 THE CYANATE-ESTER DIPOLE

2.1 Design of the Cyanate-ester Dipole

The standard method for building superconducting fragment separator magnets used at NSCL is to wind several thousand turns of superconducting wire and bind them with an high-strength epoxy like Stycast® (Emerson & Cuming, Billerica, MA). This method of building coils is cost-effective, fast, leads to high current density, and is well understood. However, even the lower radiation areas at GSI and RIA are too hazardous for coils made with this epoxy. In this work a radiation resistant cyanate-ester from CTD's 400 series, specifically CTD-422, was used to pot two 2200-turn dipole coils; the dimensions for the coils and wire can be found in Table 2-1. CTD's 400 series was chosen because it maintains high compression-strength up to 50 MGy. The wire insulation was polyimide and also had high radiation tolerance of 10^8 Gy [Ref. 8].

Prior to construction, simulations were done using Wilson's code: QUENCH [Ref. 12] in order to ensure the safety of the coils during operation (Fig. 2-1). The coil was random wound and the wire insulation was rated for 500 V per 0.0254 mm (0.001 in.). The thickness of insulation between two strands was 0.035 mm, which translated to a 689 V insulation strength. Quench voltages exceeding this could damage the coils; with a safety factor included, quench voltages below 600 V were sought.

The size and shape of the cyanate-ester coil were derived from the two small, superferric dipoles used at NSCL to steer the beam just outside the K1200 cyclotron. An example of both the cyanate-ester and the Stycast® coil are shown in Fig. 2-2. Winding methods and fixtures were already available, and the cyanate-ester coil could easily be compared to an identical NSCL epoxy coil [Ref. 4].

The field from the coil was simulated using the code POISSON [Ref. 13] (Fig. 2-3). Using various current inputs the field magnitude was calculated using POISSON. A plot of the magnetic fields and the applied current necessary to generate them is shown in Fig. 2-4. Above 2.5 T (highest conductor field) the iron saturated and the current vs. field curve raised much slower (i.e. doubling the current produced only 0.7 T more field). This curve intersected the manufacturer guaranteed short sample current curve at about 50 amps, indicating that 50 amps was the short sample current for the magnet. Because applying more current would not achieve an appreciably higher field, and because increasing the amount of copper would improve the coil's safety during a quench, the copper to superconductor ratio was set at 7:1.

Table 2-1: Wire, coil, and magnet parameters for the cyanate-ester dipole.

System	Parameters
Wire	0.445 mm diameter (bare) 0.48 mm diameter (insulated) 7:1 Cu:SC
Coil	2200 turns 25.4 x 25.4 mm cross section
Magnet	203 mm long iron 4.29 H at 51 A 5.6 kJ stored energy at 51 A

Comparison of Simulated Quench Voltages for Various Applied Currents in the Cyanate Ester Dipole

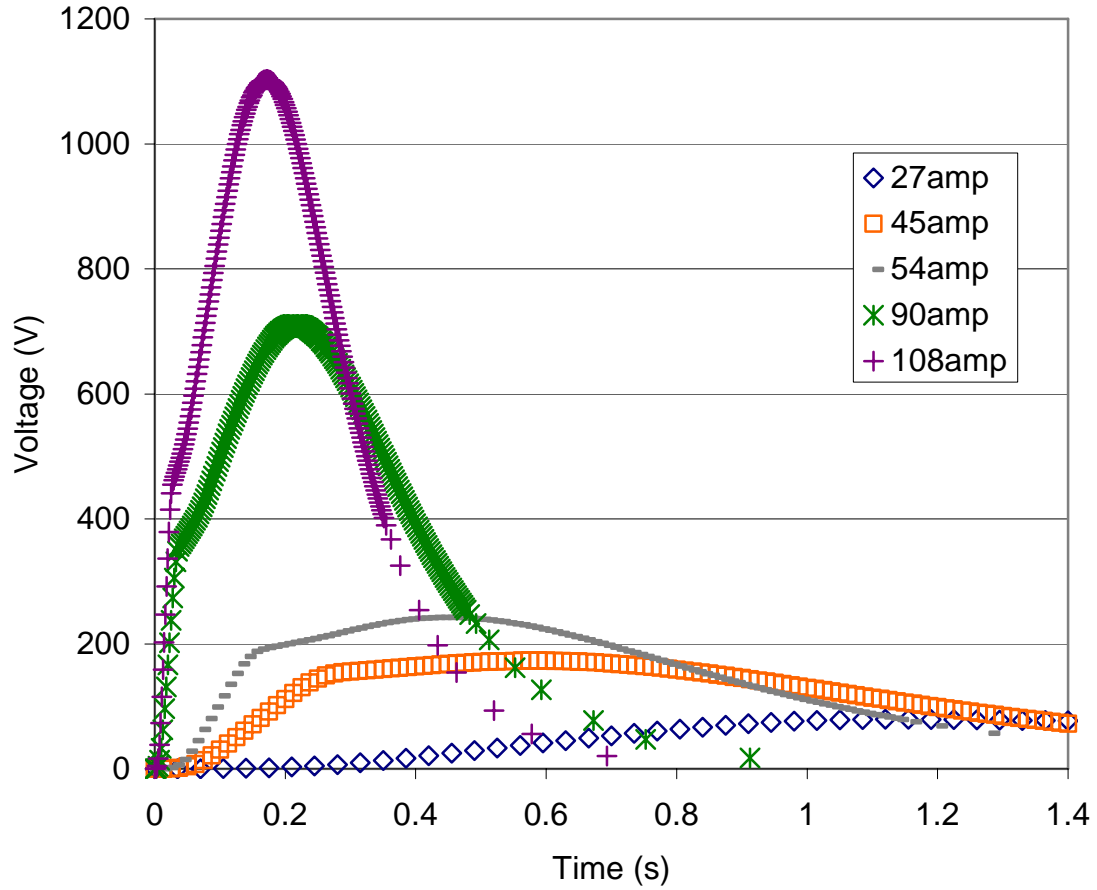


Fig. 2-1: This shows the QUENCH [Ref. 12] simulation of the quench voltages (for various currents) in the coil during a quench. The insulation around the wire was rated for 689 V (between two strands). These results demonstrate that the operating current used, which was near 54 A, would not damage the coil through arcing if a quench were to occur.



Fig. 2-2: Examples of a Stycast® epoxy-potted coil (in back) and a CTD-422 cyanate-ester-potted coil (in front).

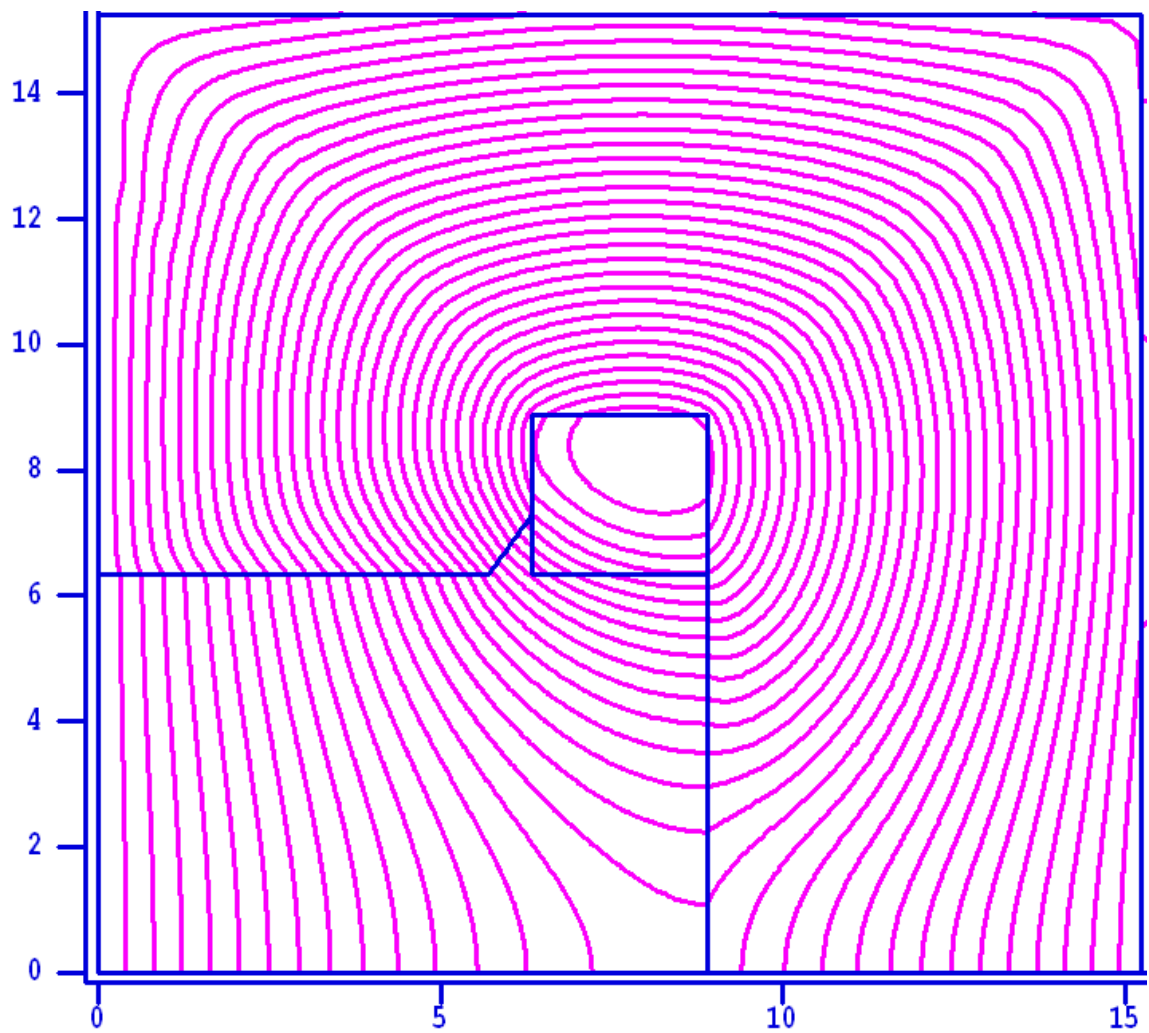


Fig. 2-3: The field lines calculated with POISSON [Ref. 13] for one symmetric quarter of the cyanate-ester dipole. The units for the x and y axis are cm.

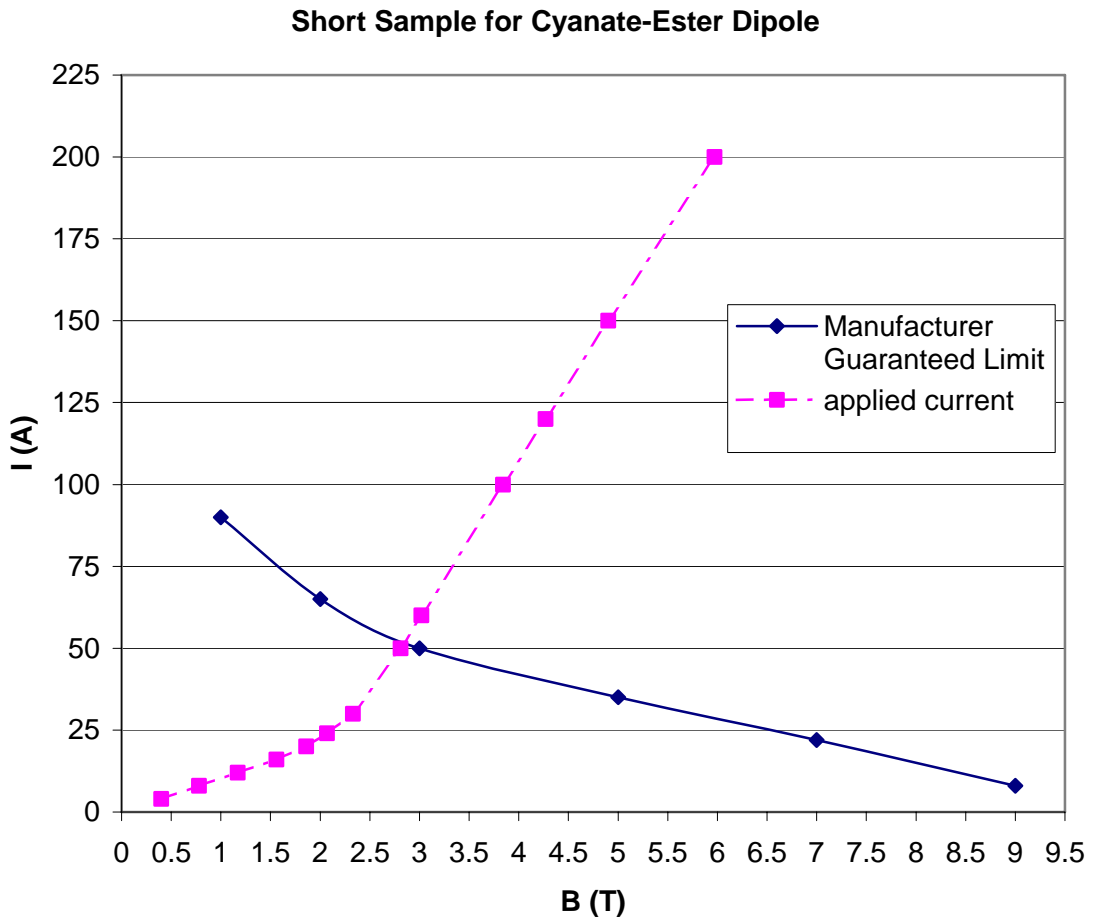


Fig. 2-4: The short sample current limit guaranteed by the manufacturer (Supercon, Shrewsbury, MA) is plotted along with the field (at the conductor) and required current calculated by POISSON [Ref. 13]. Their intersection, about 50 amps, is the estimated short sample current of the magnet [Ref. 4].

2.2 Construction of the Cyanate-ester Dipole

Magnet construction began with development of a coil winding method.

Superconducting NbTi wire with 0.48mm diameter was wrapped around a winding form to build the coils; Table 2-1 lists the wire, coil, and magnet parameters in detail. The wire was drawn through a bath filled with warm CTD-422 as it was being wound.

Difficulties encountered during the winding process led to electrical shorts inside the coil and other problems (Table 2-2). More detail about this process can be found in Appendix 5.1 and 5.2 (winding procedure and flow diagram). After exactly 2200 turns had been wound, fiberglass tape was cut to fit and then wrapped around the coil in the winding form. Form bars were then clamped to the form and the entire assembly was baked in a computer controlled pizza oven at CTD's recommended heat cycle.

The finished coils were installed into the magnet iron and shimmed in with Kapton® (polyimide) tape. Sanding and filing the iron eliminated the sharp edges that remained from the machining process. G-10 spacers were added in between the coil ends and the iron (Fig. 2-5). The spacers served to hold the coils in position when the magnet was not energized; once the magnet was energized, the field forced the coil toward the iron, and friction then immobilized the coil.

The coil leads were soldered together such that the two coils were electrically in series. The soldered leads were then fixed in place by clamping them to a post welded to the iron (Fig. 2-5). To prepare for the testing, voltage taps were also soldered to the leads.

In comparison to Stycast®, CTD-422 exhibited much greater workability and ease of use. After the CTD-422 had cured, repairs could be made by applying the

cyanate-ester over the area that needed repair, and then curing again; the bond that the cyanate-ester made to itself in repairs like this was better than the bond that Stycast® made in similar repairs. CTD-422 may need a filler to improve the viscosity because the edges of the coils were difficult to cure correctly. The solution for this problem used for the dipole coils was to wrap fiberglass tape around the coil before curing it.

Table 2-2: Problems encountered during the winding of the cyanate-ester coils

<u>Problem</u>	<u>Solution</u>
Loose turn on inner face of coil	<ol style="list-style-type: none">i. Repair by applying fiberglass tape, painting with cyante-ester, and curing again.ii. Before starting the wind, wrap a layer of fiberglass tape around the inside of the winding form.
Loose turn on outer face of coil	Machine better-fitting form bars
Rough Edges	Wrap Teflon®-coated strips around corners to give the coils a smooth and round shape
Electrical short found near end of coil	The lead wires are sensitive to damage, check for abrasion, cracks, or looseness/bad bonding.

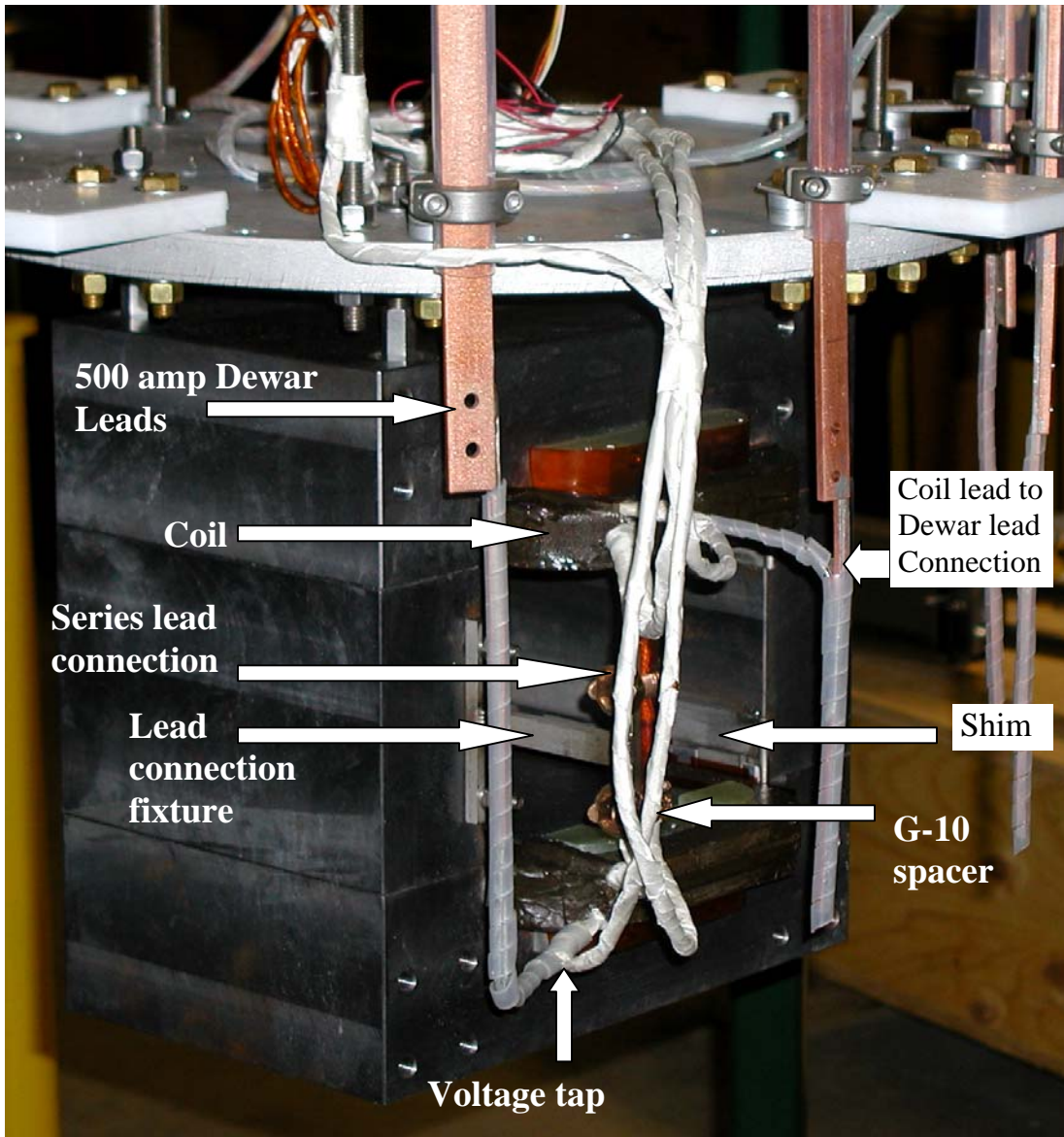


Fig. 2-5: The complete magnet assembly hangs from the Dewar lid ready to be tested. Visible are the lead connections to the Dewar leads, magnet iron, coils, G-10 spacers, and voltage taps. Partially visible are the coils shims, solder-connected leads, and solder-connected lead fixture.

2.3 Testing of the Cyanate-ester Dipole

The magnet was suspended from the lid of NSCL's dunking Dewar. The coil leads were connected to Dewar leads rated for 500 amps. An NSCL 100 A power supply was connected to the Dewar leads through a calibrated shunt that made accurate measurements of current possible. The resistance of the shunt was known, so that the current could be determined from the voltage. The Dewar was evacuated with a vacuum pump and then flushed with helium gas (called pumping and purging) in order to clean it. Liquid helium was then pumped in until the entire magnet was immersed.

During testing of the magnet the current, ramping voltage, and voltage across each coil were recorded and the results have been reported in [Ref. 4]. From the current measurements the quench history was tracked and graphed in Fig. 2-6. The magnet was able to exceed the guaranteed short-sample current on several occasions because wire manufacturers generally include a safety margin in their estimations.

The first three ramps were at 8 V and then the following ramps were at 3 V. Ramps ten and eleven were again at the full 8 V, and these showed some ramp rate dependence. While standard NSCL magnets do not exhibit ramp rate dependence, the room-temperature thermal conductivity of CTD-422 is only 2/3 that of Stycast®. If the difference in thermal conductivity also exists at 4 K, then the ramp rate dependence can be explained. The higher ramp-rate led to higher eddy-current losses, which created more heat [Ref. 4]. Poor thermal conductivity allowed heat buildup, which led to a quench.

Quench History of the Cyanate Ester Dipole Test

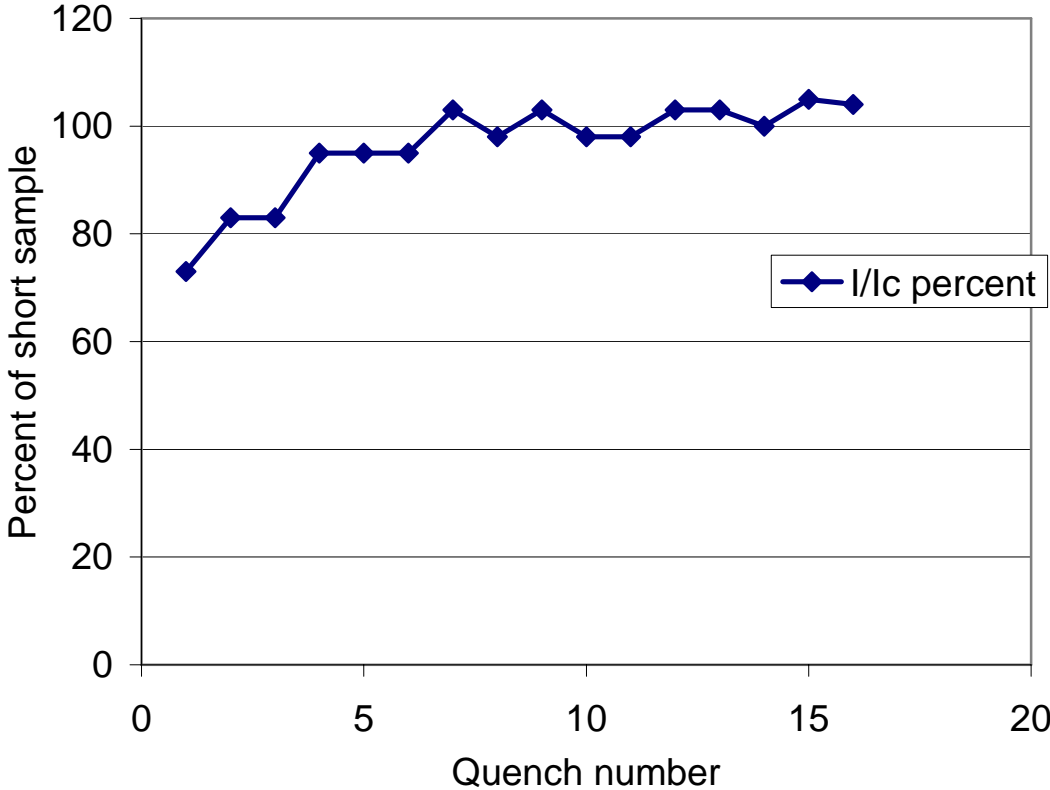


Fig. 2-6: Shown here is the ratio of applied current to short sample current (50 A) at the time of quenching [Ref. 4].

2.4 Simulation of Quench in the Cyanate-ester Dipole

The data measured in the test experiment was compared to data simulated by QUENCH [Ref. 12]. QUENCH simulates the voltage, current, temperature, stored energy, and normal volume and has given reasonable comparisons to previous magnet systems [Ref. 14].

Estimations of the transverse heat propagation velocity and the effects of iron coupling were obtained by comparing the simulation data to the experimental; the results were presented in [Ref. 4]. Fig. 2-7 shows current as a function of time and it is clear that simulations with transverse propagation velocity ratios near $g=0.015$ (1.5 %) are the best fits to the experimental current. This is considerably lower than Stycast®, which normally fits well with a $g=0.07$ (7%) transverse propagation velocity ratio [Ref. 4, Ref. 14].

Voltage simulations and measurements are recorded in Fig. 2-8. Again, the simulated 1.3% and 1.5% transverse heat propagation ratios are the best fits, and again there is little difference whether the iron is taken into account in the simulation. The first derivative of current was calculated, and matches well with the recordings for voltage (Fig. 2-9). Finally, the second time derivative of current is plotted in Fig. 2-10. The second derivative of current is used to check the agreement of the first derivative of current with the voltage; here, the inflection points and slope equal zero points are accurate. In some of these simulations the better fit is with inductively coupled iron, but the differences are not significant enough to say that the iron changes the properties of quench propagation [Ref. 4].

Current During Quench of the Cyanate-ester Dipole

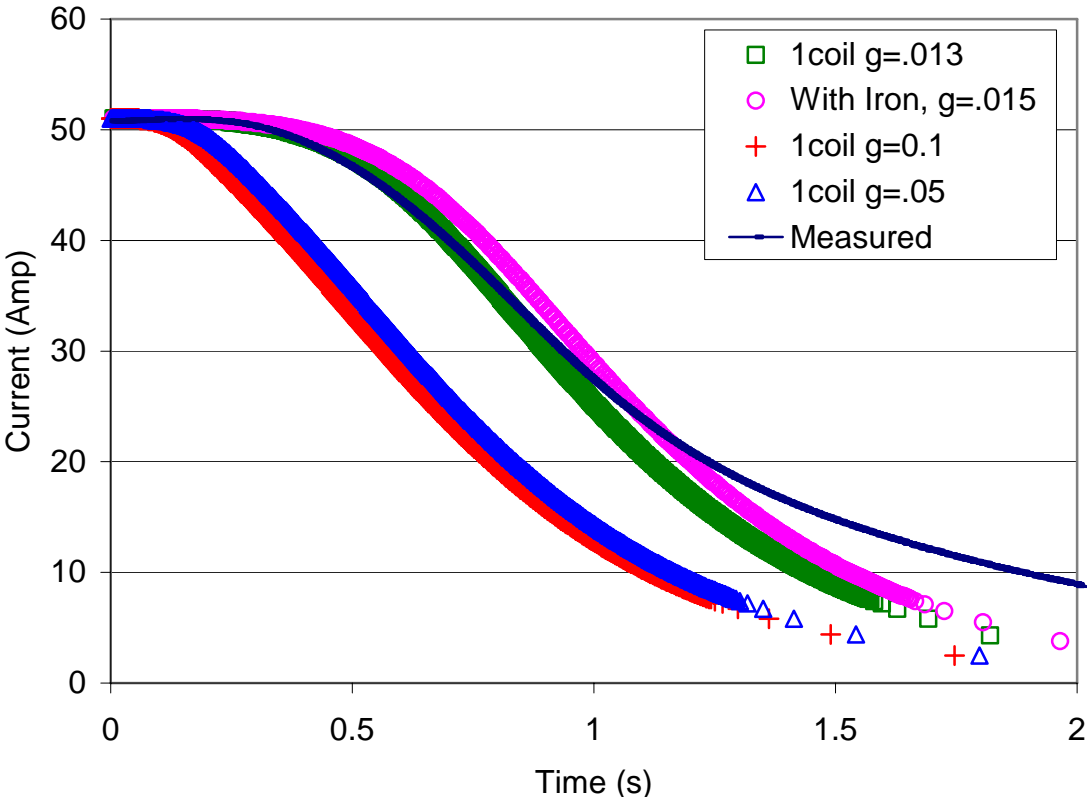


Fig. 2-7: The current measured in the cyanate-ester dipole during a quench, matched to simulation data from the code QUENCH [Ref. 12]. The best fits were for a transverse heat propagation velocity ratio of around 1.4 % ($g=0.014$). Inductively coupling the iron (denoted as ‘with iron’ above) in the simulation did not significantly vary the result. Simulations fit to Stycast®-potted coils have a transverse heat propagation velocity of about 7%.

Normalized Voltage in Cyanate-ester Dipole Quench

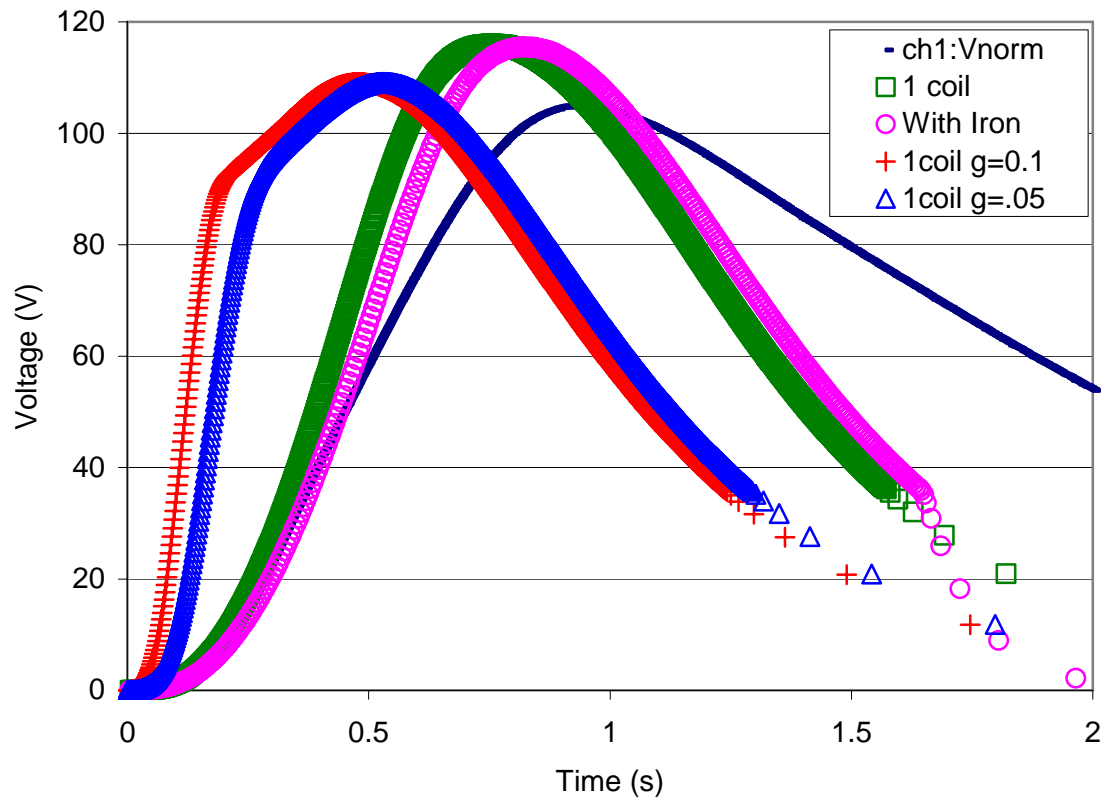


Fig. 2-8: The voltage measured in the cyanate-ester dipole during a quench, matched to simulation data from the code QUENCH [Ref. 12]. The best fits were for a transverse heat propagation velocity ratio of around 1.4 % ($g=0.014$). Inductively coupling the iron (denoted as ‘with iron’ above) in the simulation did not significantly vary the result. Voltages during the quench did not approach levels that would damage the coils.

First Derivative of Current for Cyanate-ester Dipole

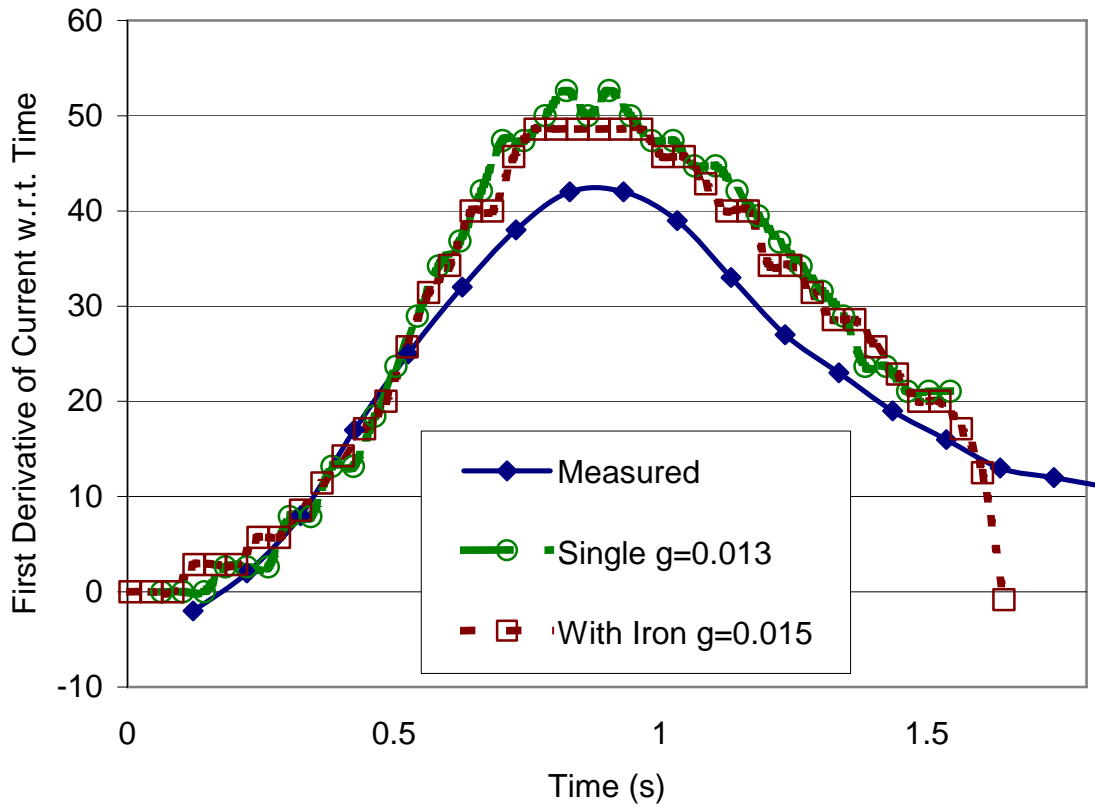


Fig. 2-9: The first derivative was calculated for the measured current and for the QUENCH-simulated current [Ref. 12]. The first derivative of current corresponds well to the voltage measurements.

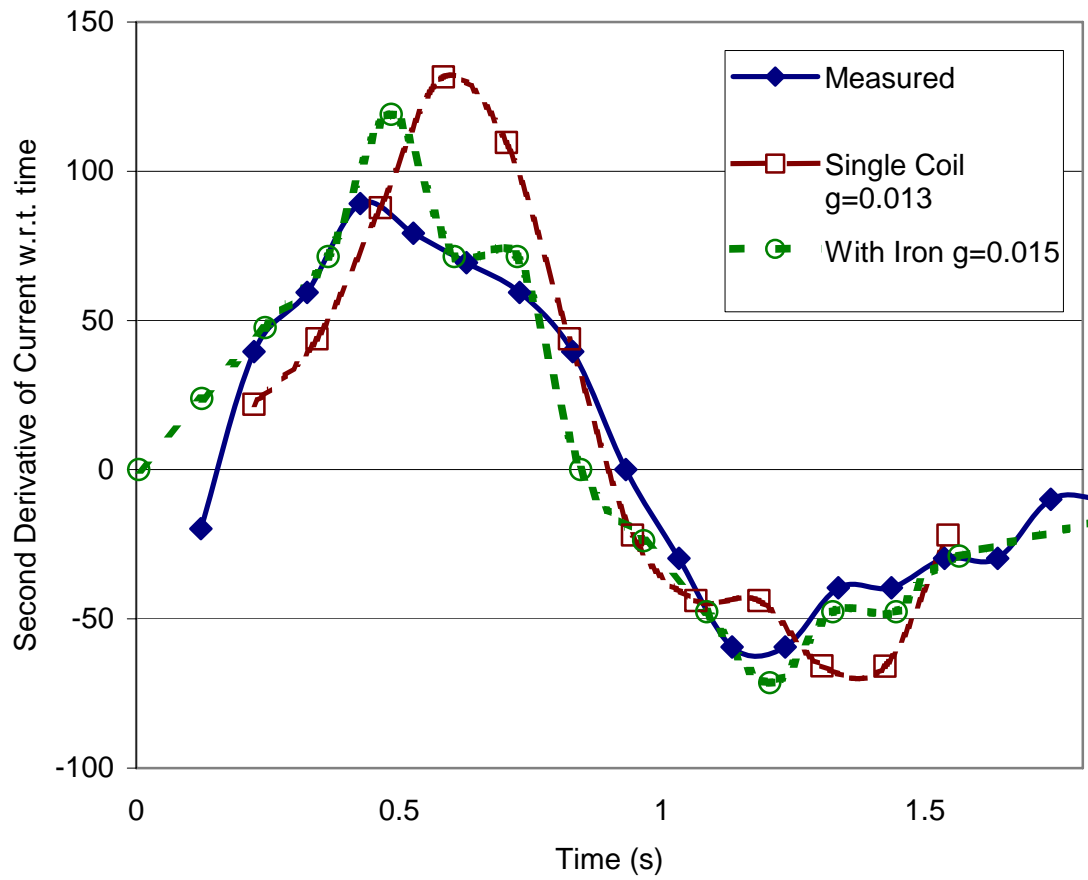


Fig. 2-10: The second derivative of current with respect to time for the quench data measured, and for two simulations from QUENCH [Ref. 12]. Inductively coupling the iron (denoted ‘with iron’) in the QUENCH [Ref. 12] input did not significantly vary the result.

2.5 Discussion of the Cyanate-ester Dipole

The CTD-422 cyanate-ester is suitable for application in the RIA fragment separator. Its advantages are its workability and higher radiation resistance than epoxy; however, high heat loads due to radiation and protecting the coil in case of a quench are of concern.

The low transverse quench propagation velocity exhibited by CTD-422 lessens its ability to produce self-protecting coils with large stored energies. An alternative active quench protection system is difficult to sustain in a high radiation environment due to the relatively low radiation tolerance of electronics. Changing the types and amounts of fillers in the cyanate-ester may improve the transverse quench propagation velocity [Ref. 4].

The low thermal conductivity of CTD-422 (compared to Stycast®) could cause problems for the stability of the superconductor. The heat generated by radiation absorption in the coil is a problem because in potted coils the conductor does not have good thermal contact with the surrounding liquid helium. The heat deposited in the conductor is approximately 2 mW/g, which is near the stability limit of NbTi. To consider the coil safe from quenching from heat, it should be used in areas with at most 1 mW/g. Therefore the coils should be placed in locations where the radiation dosage will be limited to 50 MGy or less [Ref. 4]. Also, the compression-strength of the cyanate-ester begins to significantly degrade above 50 MGy [Ref. 8]

The radiation tolerance of the magnet system has not been tested directly. The CTD-422 has been tested by itself [Ref. 15] and exhibits significant reductions in strength at dosages above 50 MGy. The radiation tolerances of the conductor are known and are

significantly higher, about $5 \cdot 10^8$ Gy [Ref. 16]. Because it is radiation resistant, irradiation of the magnet system as a whole is impractical; long irradiation times are necessary in order to notice any damage in these materials. The neutron radiation from an irradiation reactor that might be used would have a peak energy of 10 MeV; however, the average neutron energy at RIA would be above 20 MeV. In addition, because there is copper in the coils, the induced radiation may lead to problems with radioactive waste/hazard [Ref. 4].

3 THE METAL OXIDE CICC DIPOLE

3.1 Design of the MOCICC Dipole

A metal-oxide CICC dipole magnet was fabricated and tested to examine the operating properties. The primary objectives in the design of this magnet were current density and radiation tolerance.

The relationship between the amount of cold mass and absorbed nuclear heating suggests thermal separation of the coils from the iron; however, the cold-iron design is easier to fabricate for testing. For this work, a cold-iron model was developed for practical reasons; however, all development on the cold-iron model applies directly to the warm-iron model development. Forced-flow liquid helium through the inner conduit keeps the cooling central to the superconductor, and vacuum outside the coils thermally insulates them from the iron. The use of forced-flow cooling allows large amounts of heat to be convectively removed from the coils. Flow in the inner conduit would be both around the bundle and among the strands, creating a large surface area for conductive heat removal. Flowing liquid helium cools so effectively that localized heat spikes can be contained and cooled before they propagate to cause quenching.

The calculated heat load for the first quadrupole in the RIA fragment separator is 150 W in the coil mass [Ref. 17]. This heat load was simulated for the MOCICC dipole with the code GANDALF [Ref. 18], which has produced accurate simulations for other magnet systems [Ref. 19]. The simulation showed that with an input pressure of 5 atm, a mass flow of 5 g/s, and a 4 W/m heat load uniformly distributed along the 3.7 m length of conduit, the temperature rose 0.8 K [Fig. 3-1].

In order to simulate the quench behavior of the MOCICC dipole, a 0.01 s, 400 W/m heat pulse was input, using GANDALF, to the conduit in the center of the 3.7 m length. The resultant quench voltage was low (Fig. 3-2) and would not be damaging to the coil.

An increased current density could have been achieved by increasing the amount of conductor in the conduit. However, radiation heat load is proportional to density of the material, so trading liquid helium for conductor would increase the density within the conduit, and consequently increase the heat load. The ratio of the cross sectional area of conductor to void in the inner conduit is called 'fill factor'. The fill factor was set at 44% because it was difficult to insert more conductor into the conduit without special tooling, and because it represented a convenient compromise between current density and radiation heat absorbance.

The relatively small amount of stored energy in the magnet at 10 kA was 2040 J, which allowed a copper to superconductor ratio of only 2:1. Wire, coil, and magnet dimensions and parameters can be found in Table 3-1. The short-sample current limit for the wire used is about 290 A/wire or about 12 kA for the bundle.

The nominal maximum operating current for the magnet is estimated to be 10 kA because the magnet cannot operate at short sample, and because movement of the wires and subsequent heat generation are unknown for this 44% fill factor. It is important to demonstrate that MOCICC conduit with 44% fill can handle 10 kA because the required current to achieve 2.5 T field at the poletip of the first RIA quad was calculated to be 10 kA [Ref. 20].

The CICC conduit, manufactured by Tyco Thermal Controls (Trenton, Ontario Canada), was composed of outer and inner 316-stainless-steel square tubing, with a layer of dense MgO powder between them as the insulator (Fig. 1-2). The conduit manufacturing process is proprietary, but presumably the volume between the tubes was packed with MgO powder and then all were drawn into the small (1 cm) conductor dimension seen in Fig. 1-2.

MgO was chosen as the insulator because, as a ceramic, it has high radiation tolerance, and is effective as an electrical and thermal insulator [Ref. 21]. The dielectric strength of the MgO was tested by attaching a high potential generating machine, or Hipotter, to the CICC conduit; the positive lead was attached to the inner conductor, and the negative lead to the outer jacket. Voltage breakdown occurred at 5 kV, but the arcing occurred across the ends of the conduit (through air), and there was no evidence of arcing internally through the MgO. The MgO is hygroscopic, so absorbance of water from air and from condensate after cold-shocking, can degrade the dielectric at room temperature. This may cause problems in resistive magnets, but it does not affect operation at liquid helium temperatures. Quench voltages are not expected to be over 1 kV, so 5 kV is a safe margin as long as the ends are well insulated. Breakdown voltage was not tested after the coils were assembled and connected in series, and all breakdown tests were done in air, not liquid helium.

For financial and practical reasons the same iron yoke was used for the cyanate-ester magnet and the MOCICC magnet. The available space in the iron allowed only four turns in the coils. Another limitation in the number of turns was the lengths of conduit

available from the manufacturer. Only lengths of about 4 m were available for our developmental work. At larger production scales, longer lengths would be available.

Using the code POISSON [Ref. 13], the maximum field on the coil for 10 kA of current was calculated to be 2 T. The forces on the coil (per unit of depth) were also calculated to be 6.19×10^3 N/m in the x-direction and 3.76×10^4 N/m in the y-direction (axes and direction are defined in Fig. 3-4). These forces are supported in the coil by welding adjacent turns together.

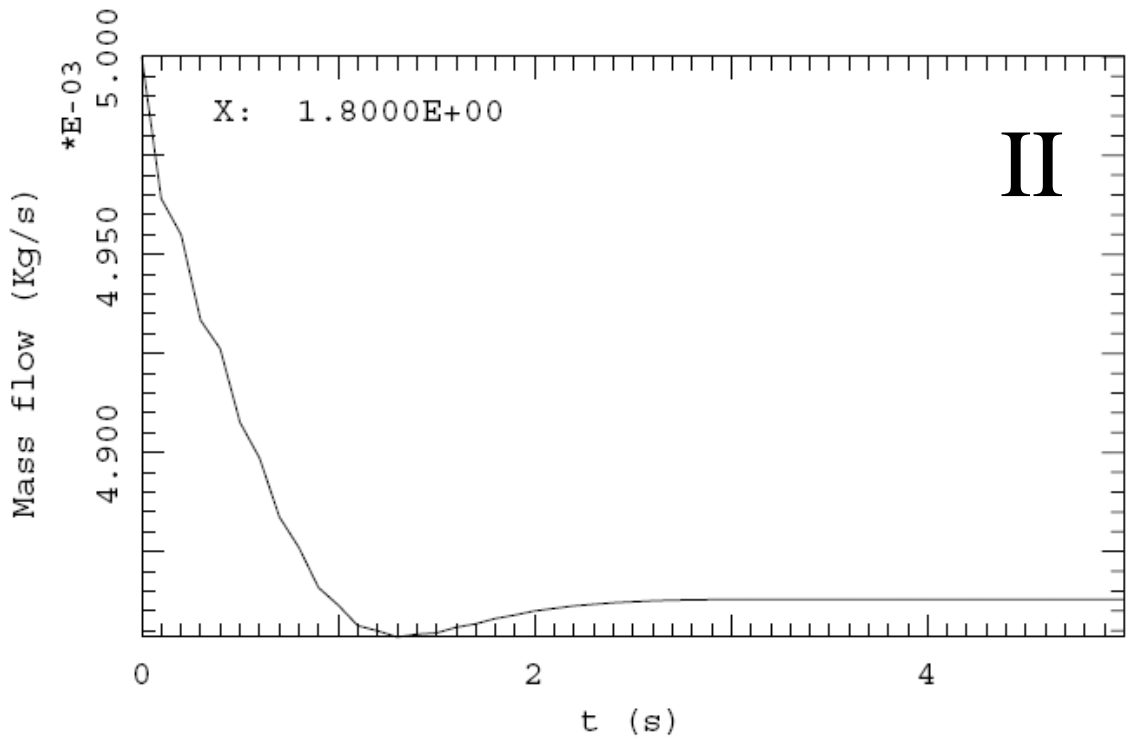
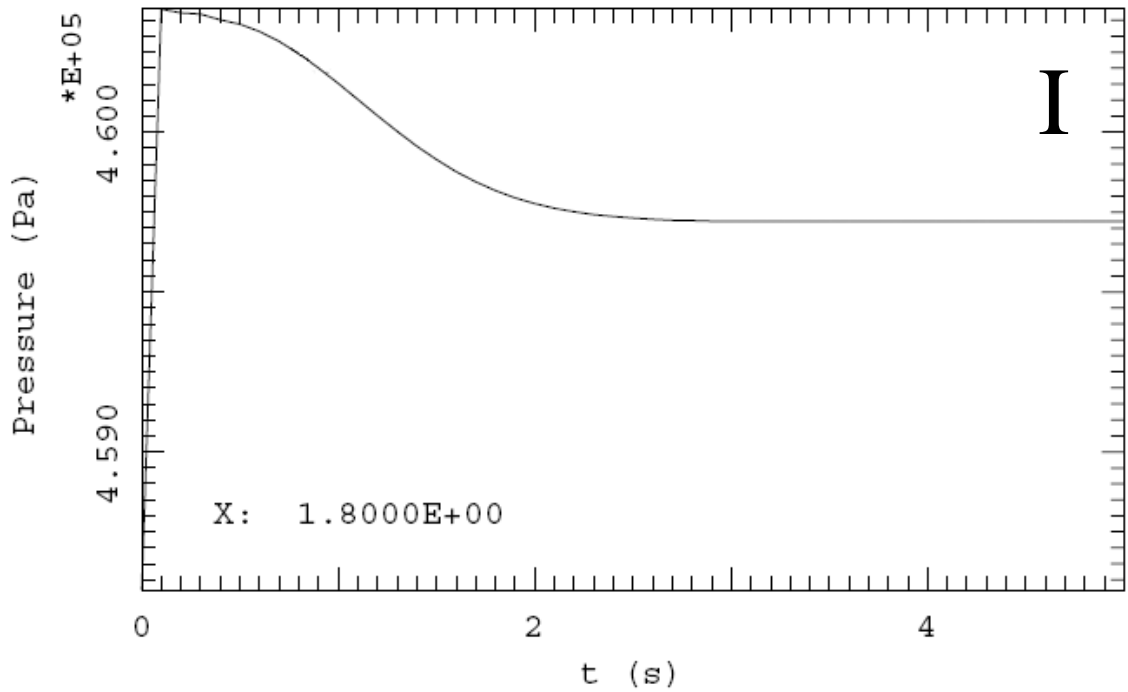


Fig. 3-1: GANDALF-simulated [Ref. 18] normal operation of the MOCICC dipole in a 4 W/m (representative of the 150 W into the first RIA quadrupole) radiation-heat load.

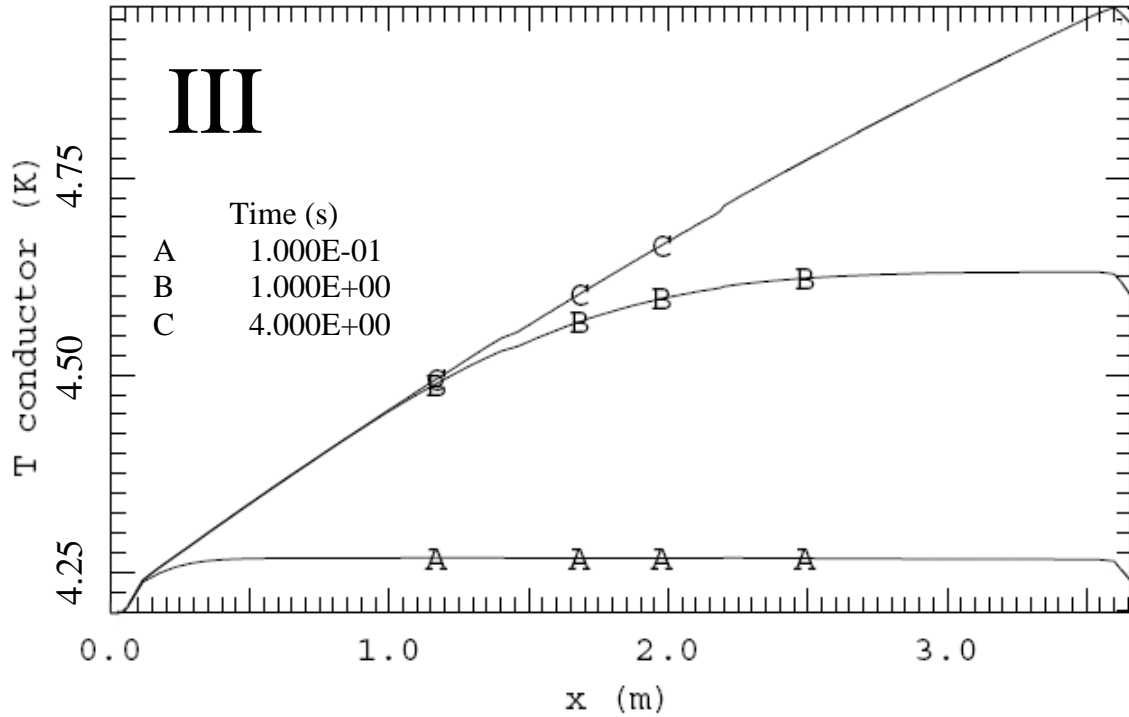


Fig. 3-1 continued: GANDALF-simulated [Ref. 18] time evolution and equilibrium of pressure, massflow, and temperature. A 4 W/m (representative of the 150 W into the first RIA quadrupole) radiation-heat load was used. The reason for the drop-off at $x=3.6$ is because the conduit ends there; the liquid helium is exiting the conduit. I) Liquid helium flow pressure reaches equilibrium around 4.6 atm (at a distance of $x=1.8$ m down the length of the conduit). II) Liquid helium mass flow reaches equilibrium at 4.87 kg/s (at a distance of $x=1.8$ m down the length of the conduit). III) Conductor temperature along the length of the conduit at times 0.1 s (A), 1.0 s (B), 4.0 s (C). The temperature profile does not change after $t=4.0$ s; curve c represents the equilibrium temperature profile along the conduit.

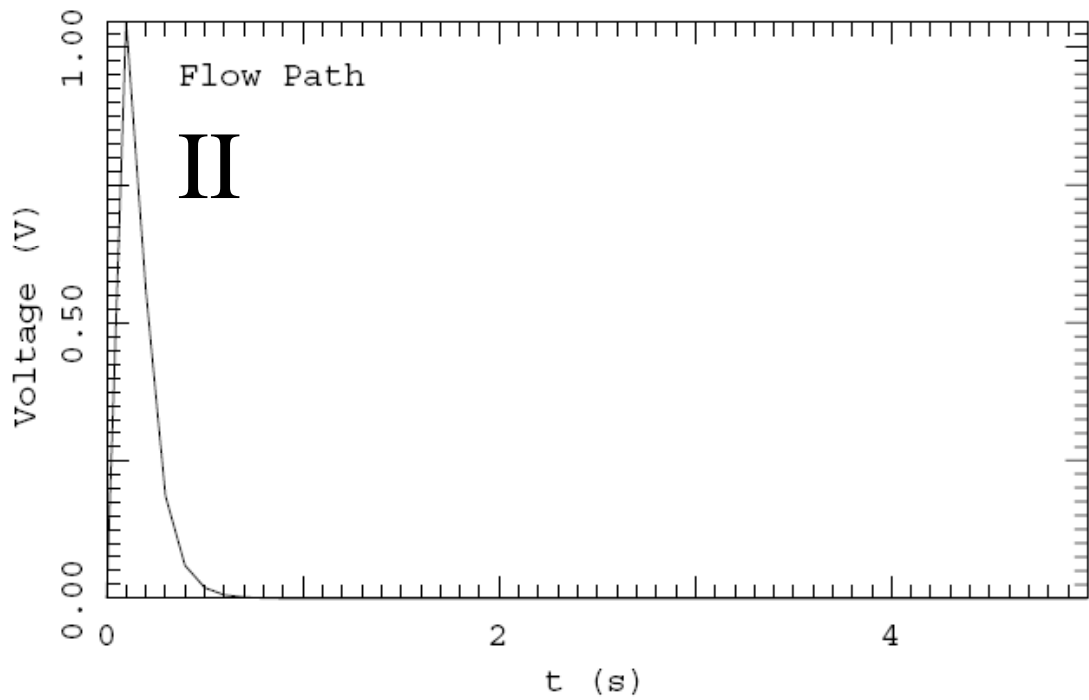
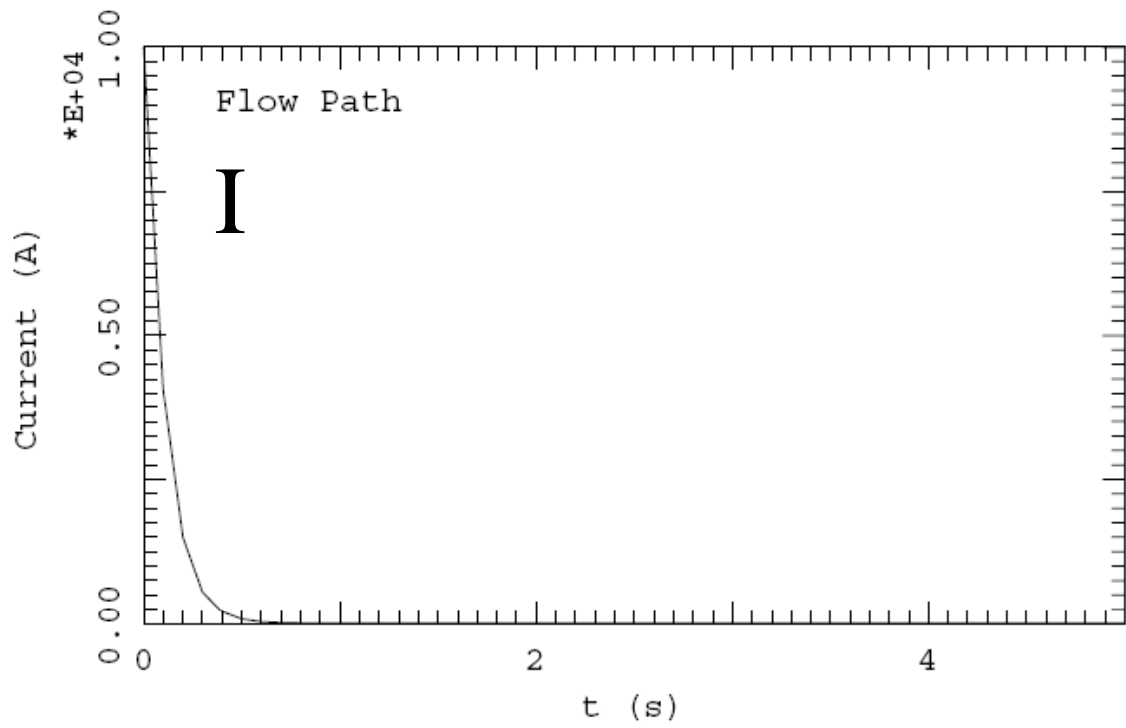


Fig. 3-2: GANDALF [Ref. 18] simulation of the propagation of a quench in the 3.7 m conduit of the MOCICC dipole.

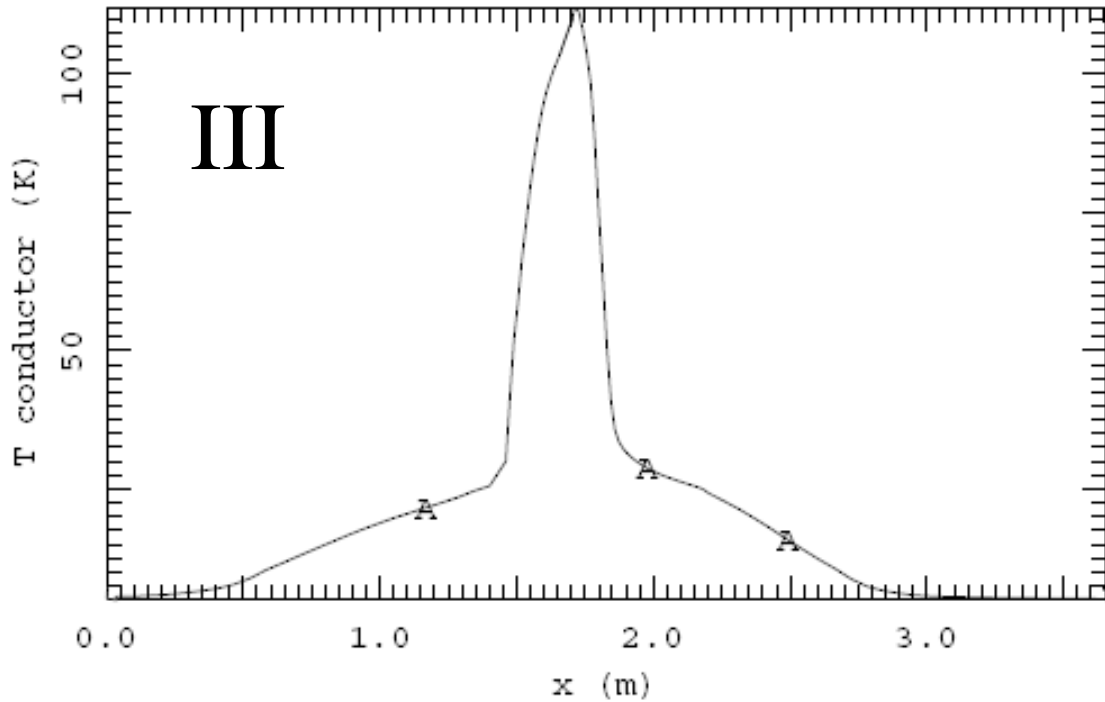


Fig. 3-2 continued: GANDALF [Ref. 18] simulation of the propagation of a quench. The quench was induced by a 400 W/m, 0.01 s heat pulse distributed from $x=1.7$ m to $x=1.8$ m in the center of the 3.6 m conduit of the MOCICC dipole. The conduit has a helium flow of 5 g/s at 5 atm. The quench lasts only 0.01 s, so the time on the graph essentially represents the time following the quench. I) The power-supply current was deactivated along an exponential decay, with time constant 0.1 s. II) Voltage between the conductor and ground (the outer stainless steel jacket) peaks at about 1 V in this quench; there is only about 2 kJ of stored energy in the magnet. III) The temperature at 0.01s (the end of the heat pulse) was not dangerous to the magnet.

Table 3-1: Magnet and Wire Parameters for the MOCICC Dipole

System	Parameters
Wire	0.5 mm diameter (bare) 2:1 copper to superconductor ratio
Bundle	42 strands (14 x 3) 44% fill factor
Coil Dimensions	4 turns 21 x 21 mm cross section 178 mm width, 192 mm length
Magnet	310 x 310 x 180 mm outer dimensions

Short Sample of 0.5mm Wire
 Data from Otokumpu NbTi 0.5mm wire filament table

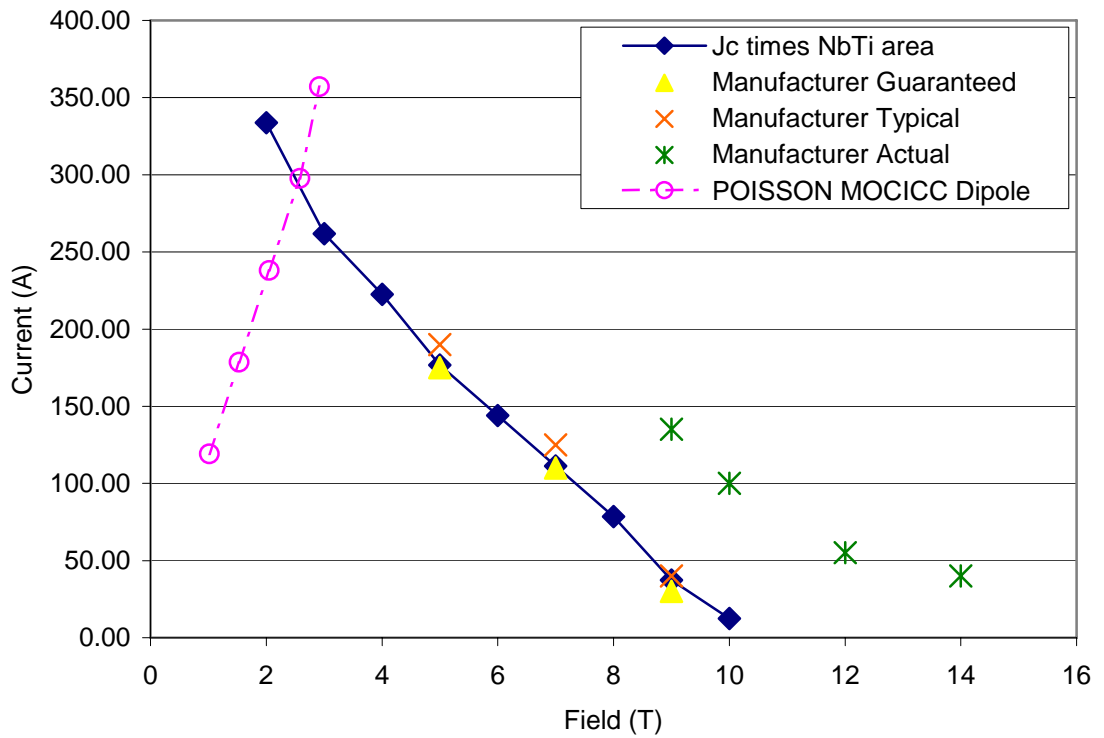


Fig. 3-3: The short-sample current limit (for the individual wire strand) is represented by the intersection (about 290 A at about 2.5 T maximum field on conductor) of the circle points, POISSON-simulated [Ref. 13] fields for given currents, and the diamond points, the critical current of the amount of NbTi material that is in the wire used (NbTi data from an Otokompu table of NbTi material properties). Also shown are the guaranteed, typical, and actual current-field specs provided by the manufacturer, Supercon.

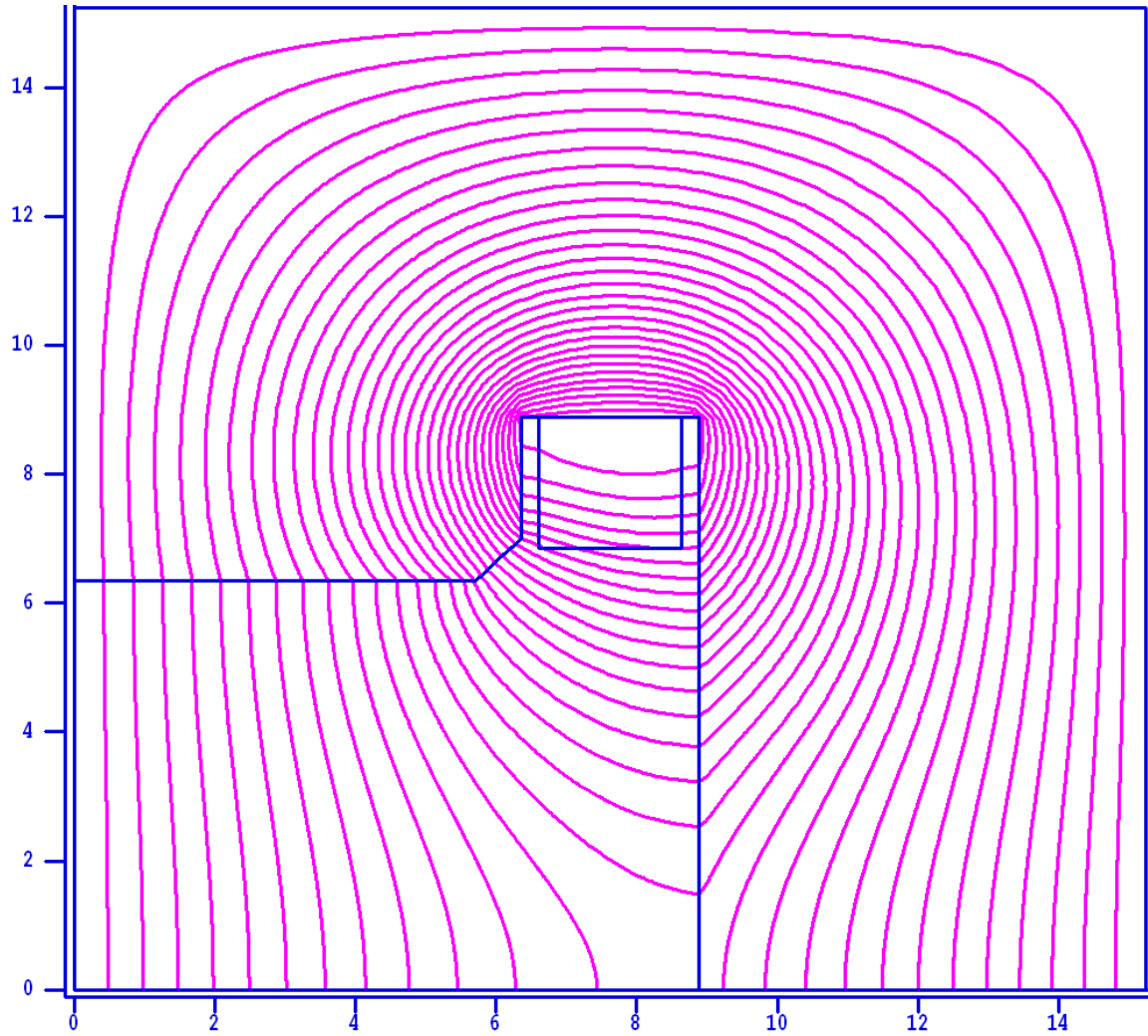


Fig. 3-4: The magnetic field lines for the top-right quarter (symmetry) of the MOCICC dipole cross-section, calculated by POISSON [Ref. 13], for 40 kA•turns. The x and y axes represent the x and y directions and the units are cm.

3.2 Constructing the metal-oxide CICC dipole magnet

The construction of the magnet consisted of winding and bundling the wire, inserting the wire into the conduit, finding the appropriate bend radius, developing a method to bend the conduit into the desired shape, welding the coils, and installing the coils in the yoke iron. Finally the leads of the two magnets were joined.

In order to create a wire bundle of appropriate length, the length of conduit needed for the 4 turns of the coil was estimated. This was done by calculating the inside and outside perimeter, averaging them, and multiplying by the number of turns. The bundle was made 450 mm longer than the estimated length of the conduit, for a total length of 4.0 m. The extra length was important to accommodate error in calculation and defects in the ends of the bundle from the cabling process.

Three lengths of conductor were wrapped onto a winding device and then spun into a small bundle that consisted of three wires. Fourteen of these 3-wire bundles were created, and again attached to the winding machine. The fourteen bundles were then spun (in the same direction as the 3-wire bundles were spun) into one large bundle of 42 wires.

The conductor wire was inserted into the conduit by hand, without the assistance of machines. The wire bundle was inserted by pulling it on one end, via a steel cable, and pushing it on the other end. The steel cable was connected to loops, on the strands at the ends of the wire bundle, which were a byproduct of the winding process. To wind the bundles, wire was wrapped around posts at opposite ends of the winder machine. The wrap around these posts created the loops. To connect the steel cable to the wire bundle, many of the bundle end-loops were cut and Teflon® tape was wrapped around the bundle

where they were cut. The 1/16" steel cable was fished through the conduit, threaded through the six remaining bundle end-loops, and then the cable was fished back through the conduit. The steel cable could then be used to pull the bundle wire into and through the conduit. However, the high friction between the conduit wall and the copper in the bundle led to problems. Sometimes, individual strands would move while the rest of the bundle did not. Other times, individual strands would kink, creating a point of very high friction that would prevent the bundle from moving. The most effective solution to these problems was the combination of pushing the bundle in at one end while pulling on the other end. The person pushing the bundle could monitor the uniformity of the pitch and watch for other signs of sliding and bunching.

Scrap lengths of the CICC conduit were used to test the effects of the bend radius on breakdown voltage. By bending the conduit with tighter and tighter radii, and then testing the voltage breakdown between the inner and outer conduit, it was determined that the integrity of the conduit's electrical insulation deteriorated with bend radii of less than 19 mm (0.75 in.). It is believed that bending the tube with small radii causes internal deformations that reduce the thickness or density of the insulation, leading to lower breakdown voltages.

To bend the conduit into the coil shape, a bending form was fabricated using four pieces of steel tubing welded to a steel plate (Fig. 3-5). A winding arm fit into the sockets on the winding plate, and then the arm could torque the conduit into the necessary shape and radii. During the winding process small tack welds were placed on adjacent turns, to retain shape and reduce the elastic potential energy of the wound steel conduit. Once the winding was complete, larger sections of weld were placed to secure the coils.

After the coils were complete they needed to be installed into the iron yoke. Normally, coils would be shimmed into the iron to prevent movement, but in this case, there was a bow in the sides of the coils (rather than being exactly rectangular, the coils were very slightly oval shaped) as a result of the winding process. When the coils were forced into place, friction due to compression of this bow held the coils in place. Once the coils were properly positioned in the iron, small steel bars (Fig. 3-6) that ran from one coil down to the coil beneath it were welded into place. These bars acted to restrain the coils in the axial direction.

Once the coils were in place, the leads were connected together with a joint, such that the coils were electrically in series. First, the wires from each magnet were soldered together. An enclosure for the soldered leads was made by fabricating two clamshell halves of a stainless steel jacket with an insulating layer of Macor® ceramic (Fig. 3-7). To complete the joint, the clamshell halves were welded around the soldered leads and around the CICC conduit. The joint was secured to the magnet iron by a post (Fig. 3-8).

The space between the square Macor® and the round soldered bundle allowed liquid helium flow for cooling the joint (Fig. 3-7). There are some areas that the Macor® insulation does not cover, where about 3 mm of liquid helium is the only insulation. The 3 mm of liquid helium should be enough to protect against the less than 1 kV quench voltages expected because the dielectric strength of liquid helium at one atmosphere is greater than 10 kV/mm [Ref. 22]. The test procedure for this magnet was to insert it into a liquid helium bath; in a device designed for actual beamline there would be liquid helium flowing through the splice area.

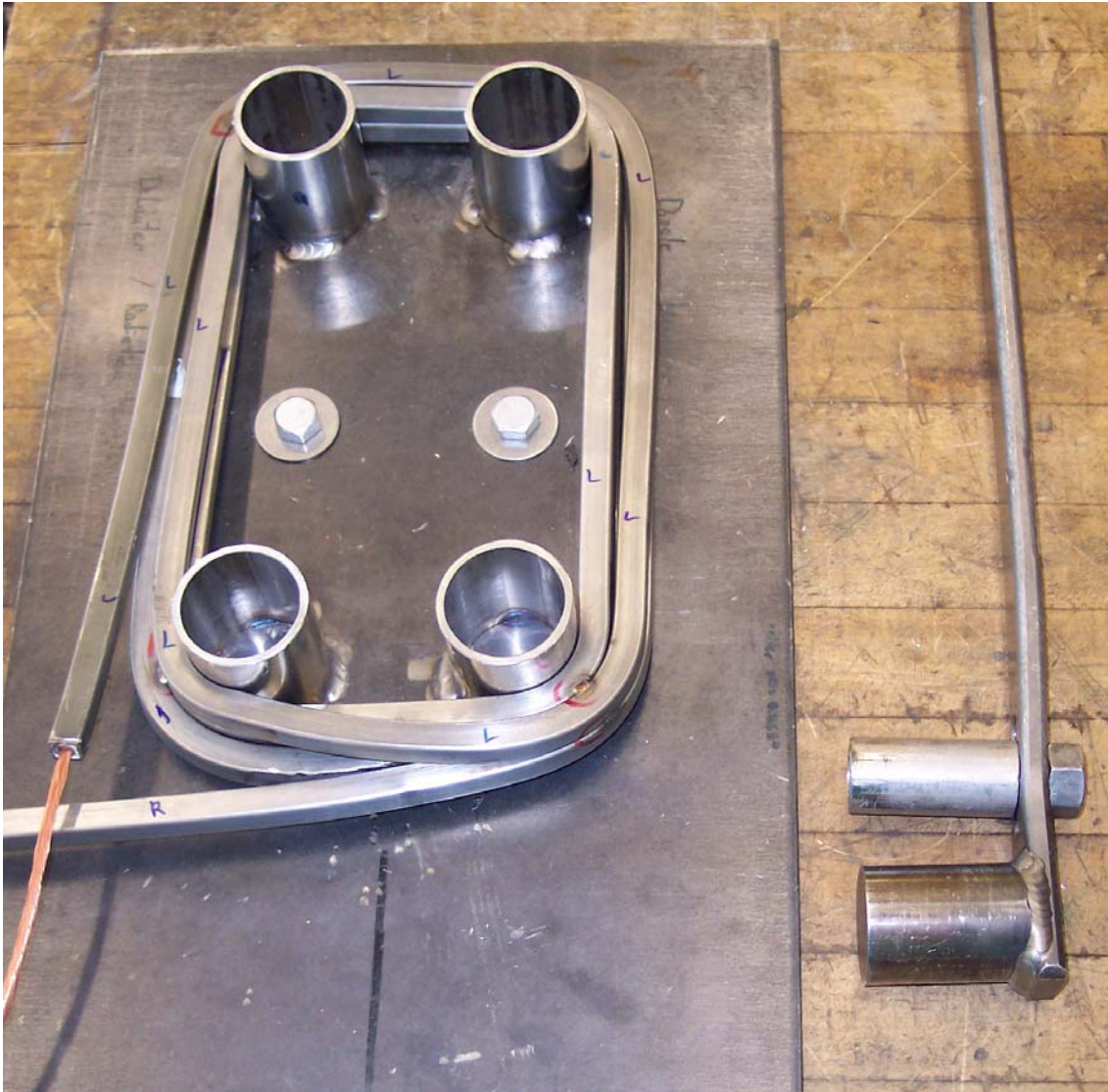


Fig. 3-5: A steel winding arm pivots inside the winding-form cylinders to wind the coil into shape. The cylinders have a 2" outer diameter and are welded onto the plate beneath them. During winding, tack welds were placed occasionally to maintain the shape.

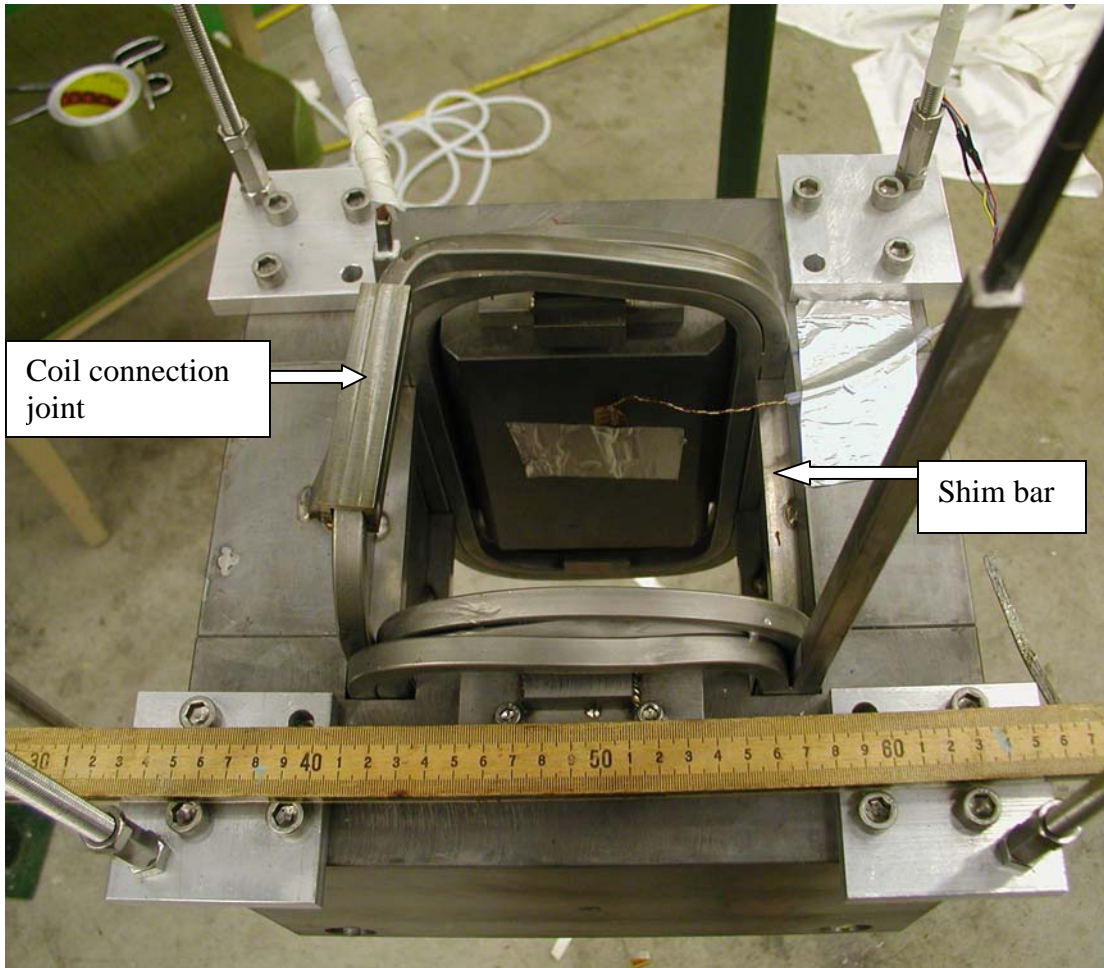


Fig. 3-6: The MOCICC dipole hangs from the NSCL Dewar lid, ready to be tested. On the left is the lead connection between the two coils.



Fig. 3-7: The joint that connects the coils in series is comprised of the solder wire bundle surrounded by two clamshell halves made of an outer stainless steel jacket with a Macor® insert to prevent the conductor from making contact with ground. Seen here is a cutaway: one of the two clamshell halves.

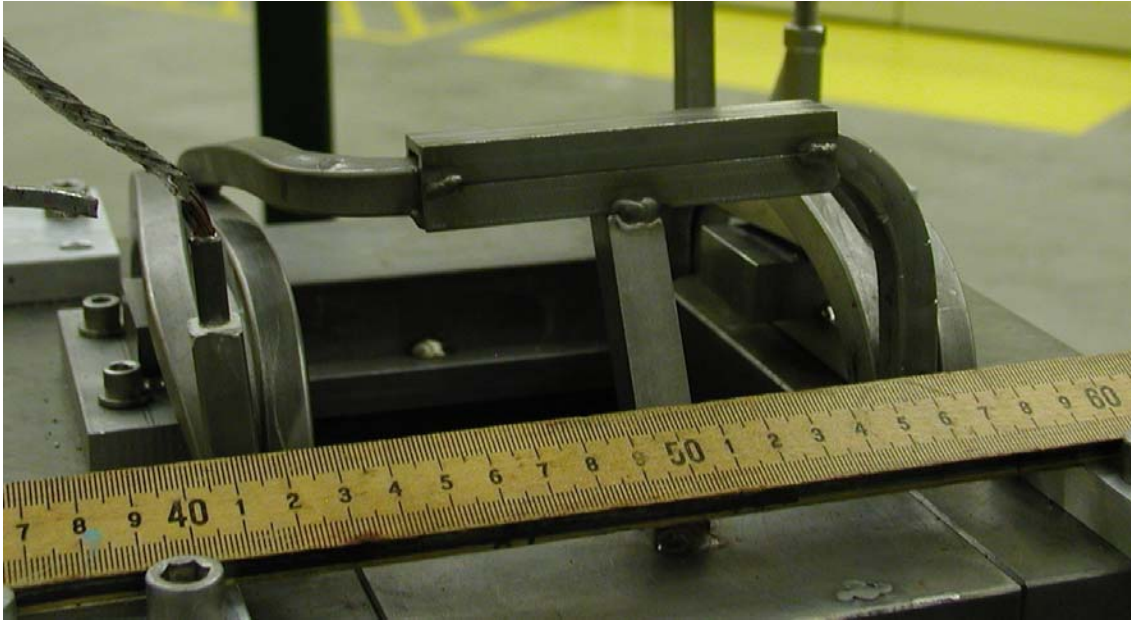


Fig. 3-8: The completed lead connection joint is seen here, secured to the magnet iron by a post. The two clamshell halves were welded in place around the soldered bundle.

3.3 NSCL Test Results

The metal-oxide CICC dipole magnet was tested at the NSCL. The NSCL's available power supply, a 1200 A PowerTen (subsidiary of Elgar, San Diego, CA) power supply, model P63C81200, limited the test to 1200 amps. The test was simple and served mainly to confirm that MOCICC technology can be used to produce superconducting magnets.

The complete magnet was mounted under a Dewar lid, where the magnet leads were connected to 1000-amp-rated leads in the Dewar lid (Fig. 3-9). The Dewar lid and magnet were lowered into the Dewar, which was then sealed, evacuated, subjected to a pump-and-purge purification process, and then filled with liquid helium. It was necessary to maintain the level/height of the liquid helium above the top of the magnet in order to keep the superconducting coils immersed. Although MOCICC technology was designed for forced-flow liquid helium, instead a liquid helium bath was used for this test. The 1200 A NSCL power supply was connected to the 1000-amp-rated leads.

The magnet ramped to 1200 A at 1.2 V in about 1 minute in two tests. At this current the magnet was stable and did not quench. The 1200 A current used in this test was only a small fraction of the predicted sustainable current: 10,000 A. To gather more information on the current density and other operating properties, another test was done at the Massachusetts Institute of Technology's (MIT) Plasma Science and Fusion Center with a 10,000 A power supply and more extensive instrumentation.

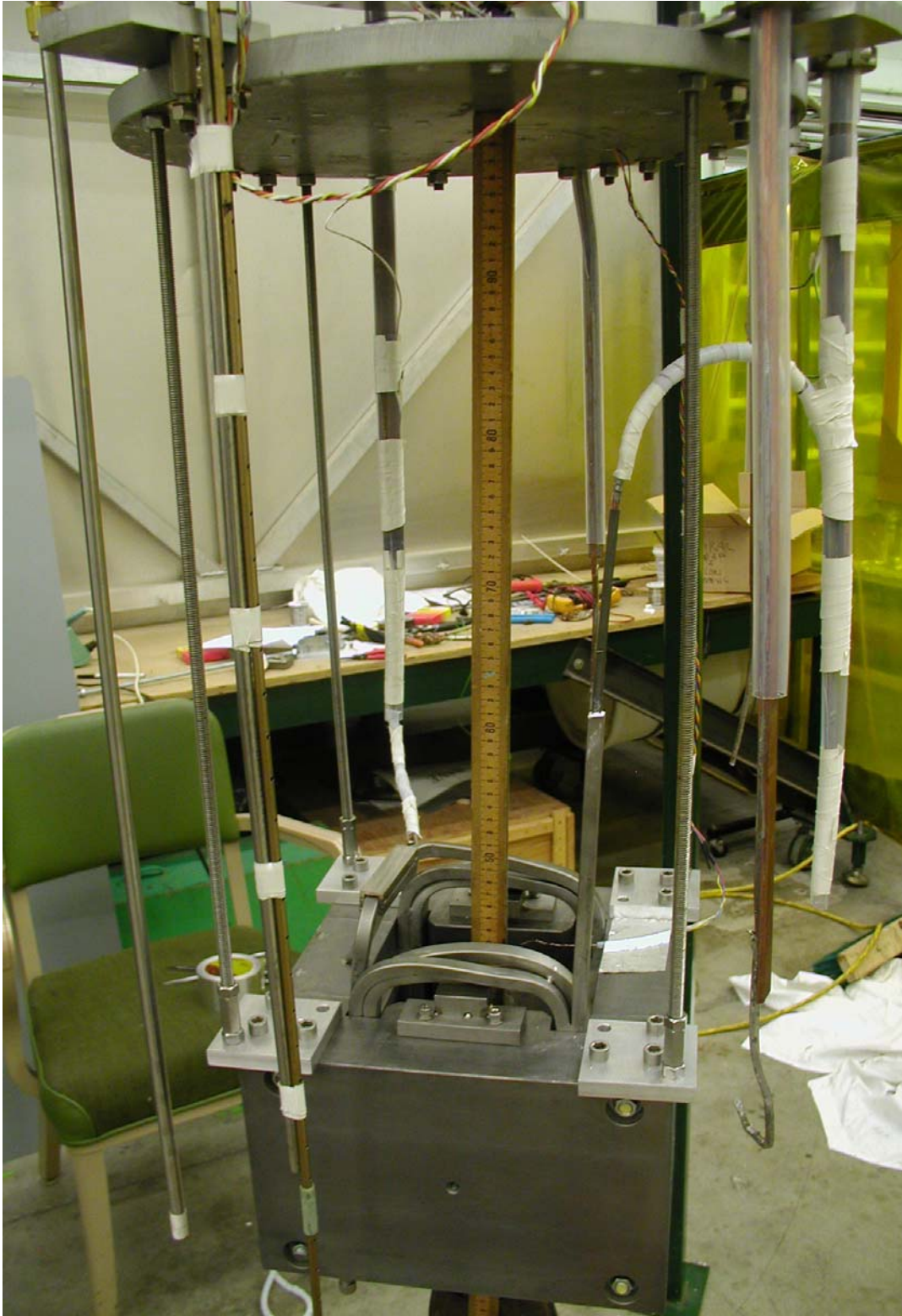


Fig. 3-9: The MOCICC dipole hangs under the NSCL dunking Dewar lid, ready to be tested. The magnet leads have been connected to the Dewar leads.

3.4 October 2006 MIT Test Results

The MOCICC dipole was shipped to MIT, where it was installed into a Dewar and prepared for testing. One of the magnet leads was connected to 10 kA helium gas-cooled Dewar leads through a superconducting Rutherford cable lead bridge (Fig. 3-10). The Rutherford Bridge was soldered to the magnet lead, and connected to the Dewar lead by two copper blocks that bolted together to fix it in place (Fig. 3-11). The other lead was simply clamped to the block. To prepare the Dewar for the test, it was cooled with liquid nitrogen, evacuated, filled with liquid nitrogen, pumped free of liquid nitrogen, and then filled with liquid helium. Nearly 300 L of liquid helium were needed to fill the Dewar to the desired 50% level (Fig. 3-12).

The magnet was powered by a Dynapower 10 kA, 20V supply, and was protected by a quench protection circuit, which would trip the power supply at a voltage and time delay set by the user. To record the test results, the Dewar instrumentation was connected to both a Macintosh computer and a Yokogawa LR8100 8-channel data recorder. In addition, three digital voltmeters measured power supply current, power supply voltage, and induction coil voltage (respectively from top to bottom in Fig. 3-13).

The magnet, first ramped at 100 A/s, quenched at 2750 A. The lead connection denoted V1_a in Fig. 3-12 showed a great deal of noise (Fig. 3-14), probably from wire movement, as the lead was not restrained well. Voltage spikes due to noise from wire movement are common in accelerator magnets, and this was likely the cause of the premature quenching. The other lead connection denoted V1_e in Fig. 3-12, had resistive voltage, but on a smaller scale than the noise found in V1_a.

The quench protection circuit delay and the ramp rate were increased, and it was found that by increasing the ramp rate, more current could be applied to the magnet coils before the Rutherford bridge quench heat propagation would reach the magnet and initiate a quench in the magnet. The results of this procedure are in Fig. 3-15 and the maximum current attained was about 4320 A. A faster-sampling voltmeter read a peak current of 4500 A, suggesting an uncertainty of about 180 A in the peak current measurement.



Fig. 3-10: MOCICC dipole magnet ready to be inserted into MIT's Dewar. The large Dewar leads are helium gas cooled.

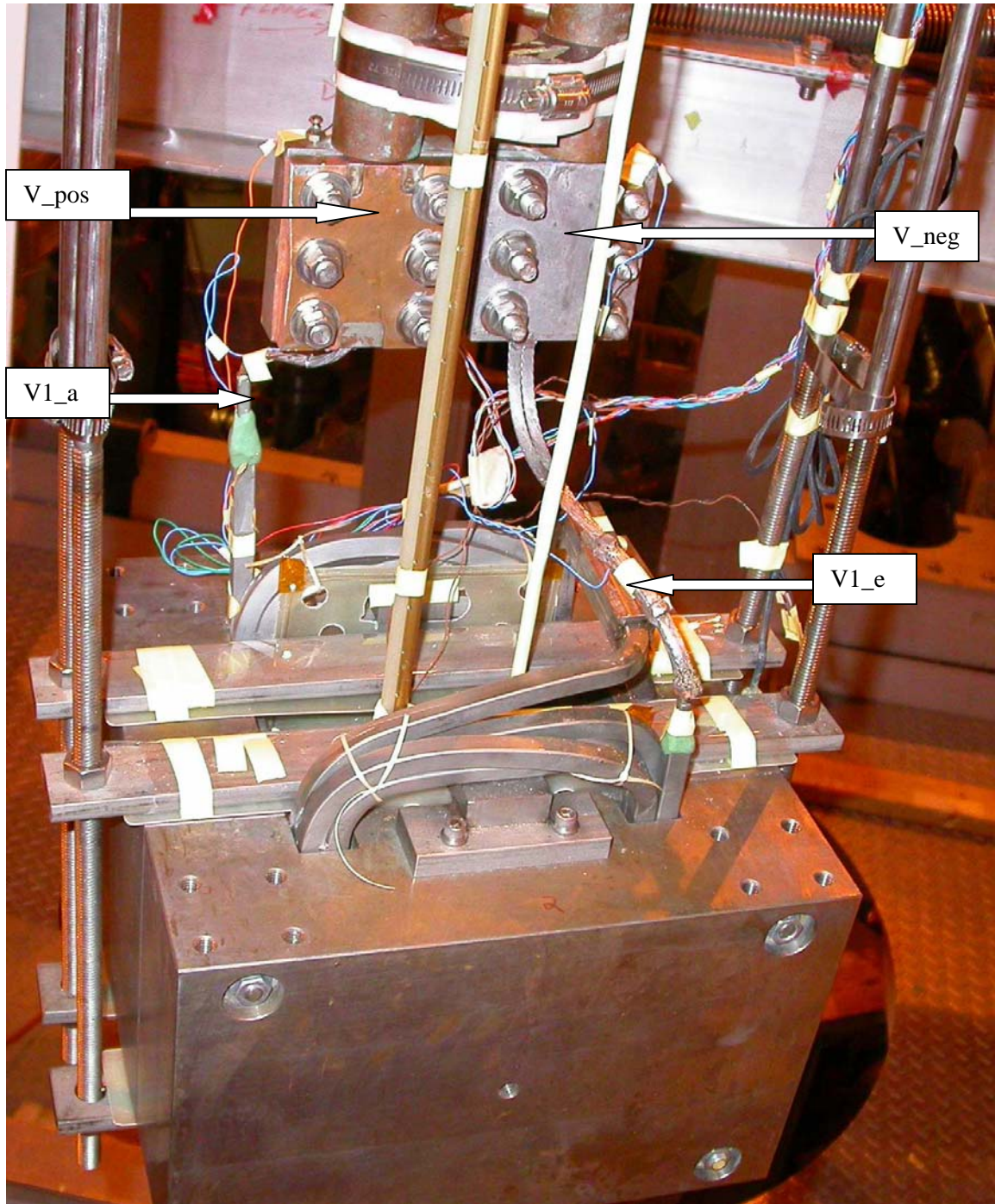


Fig. 3-11: Close-up view of the lead connections. The short magnet lead on the right is connected to the Dewar lead by some clamped Rutherford superconducting cable, which quenched during the testing. Labels have been applied that correspond to the diagram in Fig. 3-12.

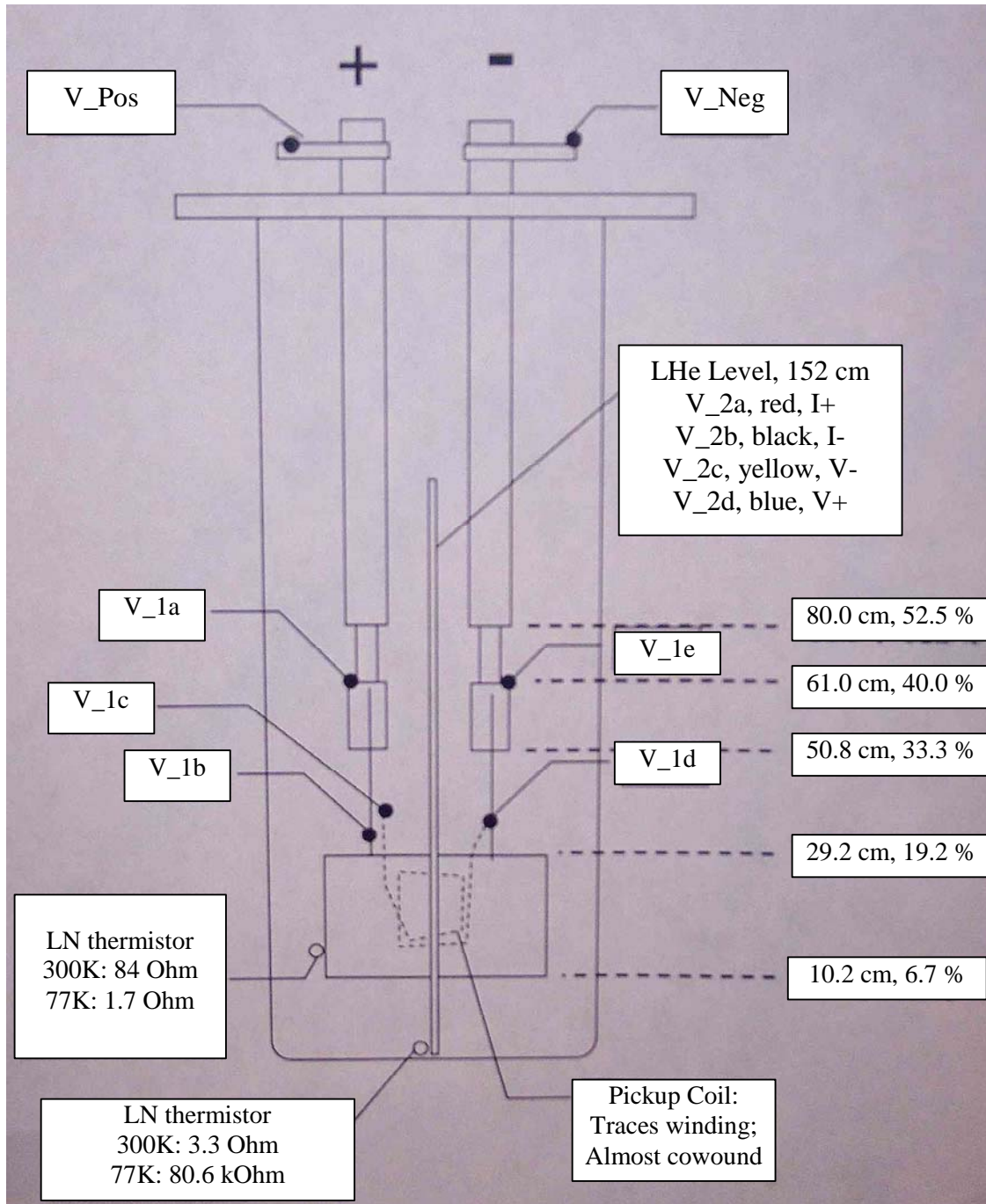


Fig. 3-12: Diagram of the test instrumentation inside the Dewar. V_1a and V_1e are voltage taps on the left and right (respectively) connections between the Dewar leads and the magnet leads. V_1c and V_1d are voltage taps a nearly-co-wound coil for measuring induced voltage. V_1b is a voltage tap to measure the magnet voltage. The liquid helium level sensor instrumentation is labeled V_2a through V_2d. On the right hand side of the diagram are the liquid helium levels needed to reach the specified heights in the Dewar; a height between 40% and 50% was desired.

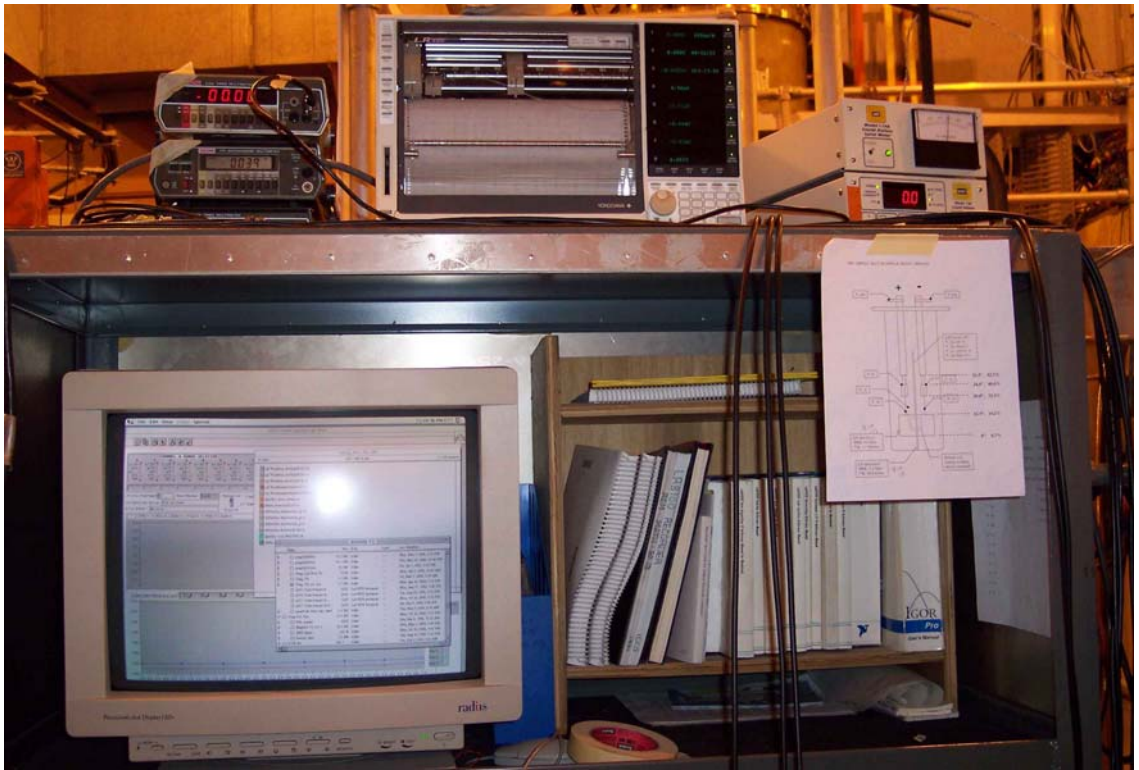


Fig. 3-13: The instrumentation setup at MIT. Data were recorded by a Macintosh computer (bottom left), a Yukagawa LR8100 8-channel data recorder (top), and three digital voltmeters (top-left).

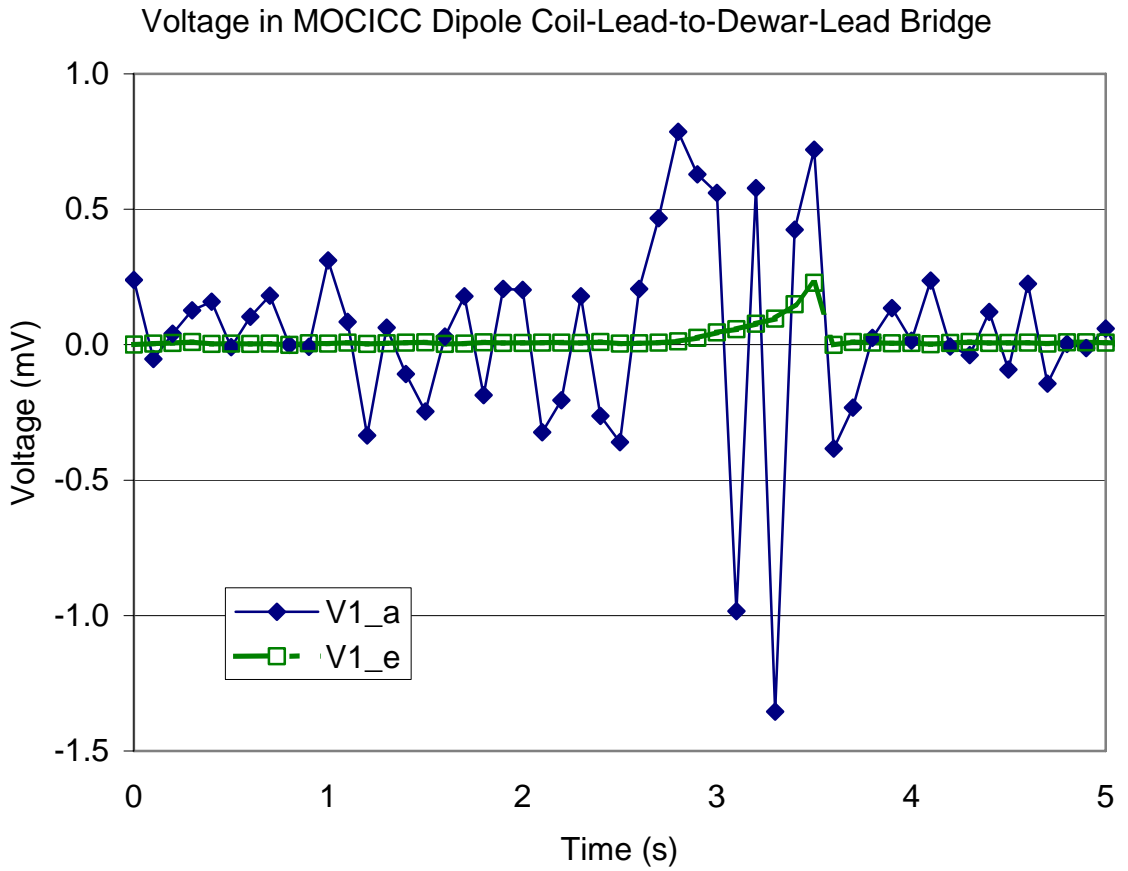


Fig. 3-14: Measurements during the ramp-up of the magnet (ramp #5 according to Fig. 3-15) from the voltage taps V1_a and V1_e (labeled according to Fig. 3-12), the bridge connections between the coil leads and the Dewar leads.). V1_e begins to generate resistive voltage shortly before the quench (the quench occurred after 3.5 s) and V1_a is very noisy during the entire ramp. The magnitude of the noise on V1_a is much higher than the resistive voltage on V1_e. It is likely that the noise on V1_a was generated by wire movement, and was the cause of the premature quench of the magnet. The ramp rate for this test was 700 A/s. The other tests, at various ramp rates, showed similar results.

Quench History for Oct. MIT Test
 Labels represent quench number

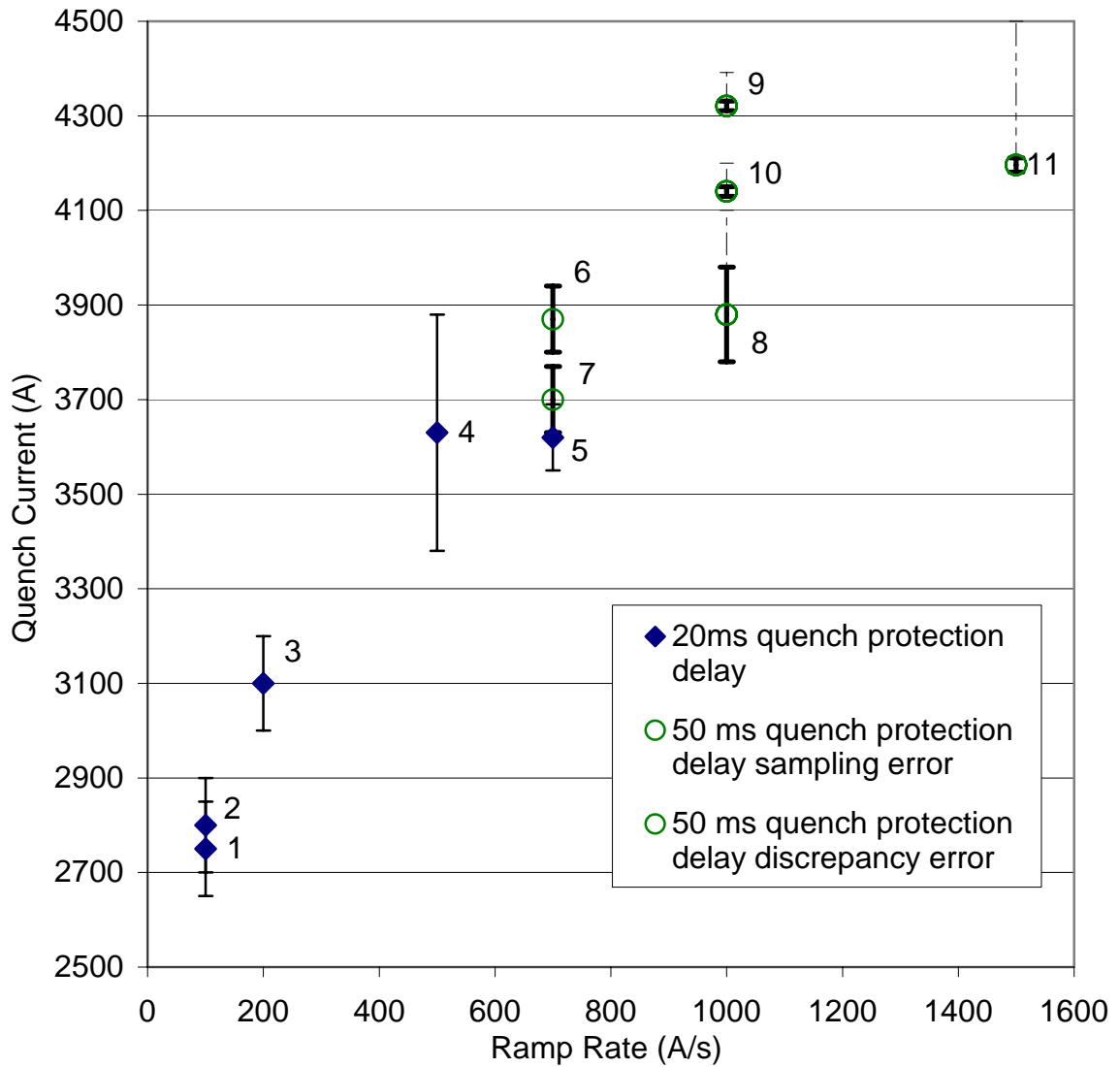


Fig. 3-15: Quench history of the MOCICC dipole test at MIT. The magnet could not be ramped to its full sustainable current due to problems with the connection between the Dewar leads and the magnet. By increasing the ramp rate, the magnet current could be pushed farther before heat propagating from the quench in the lead connection would initiate a quench in the magnet. Error in the measurement due to sampling rate is shown with thick, solid error bars. For the last four measurements, the measurement was read from voltmeters, which did not agree with the measurement read by the computer. This discrepancy is represented by light, dotted error bars.

3.5 Analysis:

The successful ramp test at the NSCL demonstrated the first step in producing a scalable superconducting MgO CICC magnet with radiation resistant materials. The 1200 A applied current was only a small fraction of the maximum sustainable current, but the test was significant as proof-of-concept for the new technology, and established its ability to carry an effective current of over 12 A/mm^2 .

The importance of the result is that the MgO CICC technology is scalable to larger devices. The entire MgO CICC conduit can be scaled up in size, without changing the thickness for the MgO layer or the steel jacket. This would create more room for conductor and reduce the fraction of the overall cross section that the non-conductor components occupy. Other research into magnet technologies with radiation resistance at the 10^8 Gy scale has produced small coils, with anodized aluminum or with ceramic-sheet-insulated turns [Ref. 23], but these technologies cannot be straightforwardly scaled up to the size necessary for fragment separators.

Scaling the size of the CICC to achieve higher current density has the consequences of higher operating current and more absorbed radiation heat. Absorbed radiation heat is related to the density of the material; therefore, exchanging liquid helium for copper/NbTi leads to an increased heat load. Increasing the size of the CICC and hence the size of the conductor would require an increased operating current in order to achieve larger current density.

Flaws in the connection from the Dewar leads to the magnet leads prevented the magnet from ramping to the full 10 kA desired. By increasing the ramp rate to circumvent the bridge connection, a current of 4.3 kA was achieved. The 4300 A applied

current translates to an effective current of 43 A/mm^2 . Resistive mineral-insulated-conduit, the only other scalable magnet technology with 10^8 Gy radiation tolerance, has current density on the order of 2 A/mm^2 ; therefore, 43 A/mm^2 is a significant step forward in radiation-resistant magnet research.

3.6 Further Research

The MOCICC can be improved to achieve higher current densities. The manufacturer of the conduit claims that the thickness of the outer stainless steel jacket, the MgO insulation layer, and the inner stainless steel jacket can all be reduced to 0.5 mm. This would reduce the overall cross section, and greatly improve the effective current density. This approach could lead to a current density of up to 170 A/mm^2 . Another means of improving the current density would be to 'co-draw' the conductor with the conduit. The conduit starts as larger tubing and is drawn down to the 1 cm size; by inserting the conductor before this is done, a much greater packing factor can be attained. The forces involved in the co-drawing process may damage the superconducting filaments in the wire, so testing is necessary; a sample of co-drawn MOCICC is awaiting testing at Brookhaven National Lab.

Changing the MOCICC insulation material may also improve its dielectric performance. Spinel (MgAl_2O_4) is another radiation resistant ceramic that has a better dielectric insulation, better radiation tolerance, and resulted in higher arcing voltages when tested (the sample had 30% spinel and 70% MgO) [Ref. 5]. Spinel appears to be less hygroscopic than MgO, but at liquid helium temperatures water would freeze and no longer affect the dielectric strength.

Constructing the conduit with aluminum jackets, rather than stainless steel, might also improve the radiation tolerance. Because of its lower density, the aluminum would absorb less radiation heat. In tests, welding aluminum jacketed, Al_2O_3 -powder insulated MOCICC resulted in a significant, although non-damaging temperature rise. The Al_2O_3 also showed a lower breakdown voltage than MgO, but the arc voltage was still much

greater than the expected quench voltages [Ref. 5]. Unfortunately, the weld size for aluminum is much greater, leading to a larger overall cross section, and a smaller effective current density.

In order to test the stainless steel MOCICC at higher magnetic field strength, and also to confirm the scalability of the technology, a large quadrupole is in development at NSCL. The quadrupole will consist of multiple coils, and a standardized method of connecting coils will be developed.

4 CONCLUSIONS

The technology now exists to build next generation fragment separators with radiation resistant superconducting magnets. Metal-oxide insulated CICC magnets can provide relatively high current densities with materials tolerant of radiation on the order of 10^8 Gy. This will be useful for applications like quadrupoles, where the current density requirements make resistive mineral-insulated magnets an unpleasant option. Cyanate-ester potted magnets can be used in areas on the order of 10^7 Gy, and will be useful for fragment separator magnets that are not directly following the target. Both technologies may have further applications, such as magnets for fusion research.

5 APPENDICES

5.1 Cyanate-Ester Winding Instructions

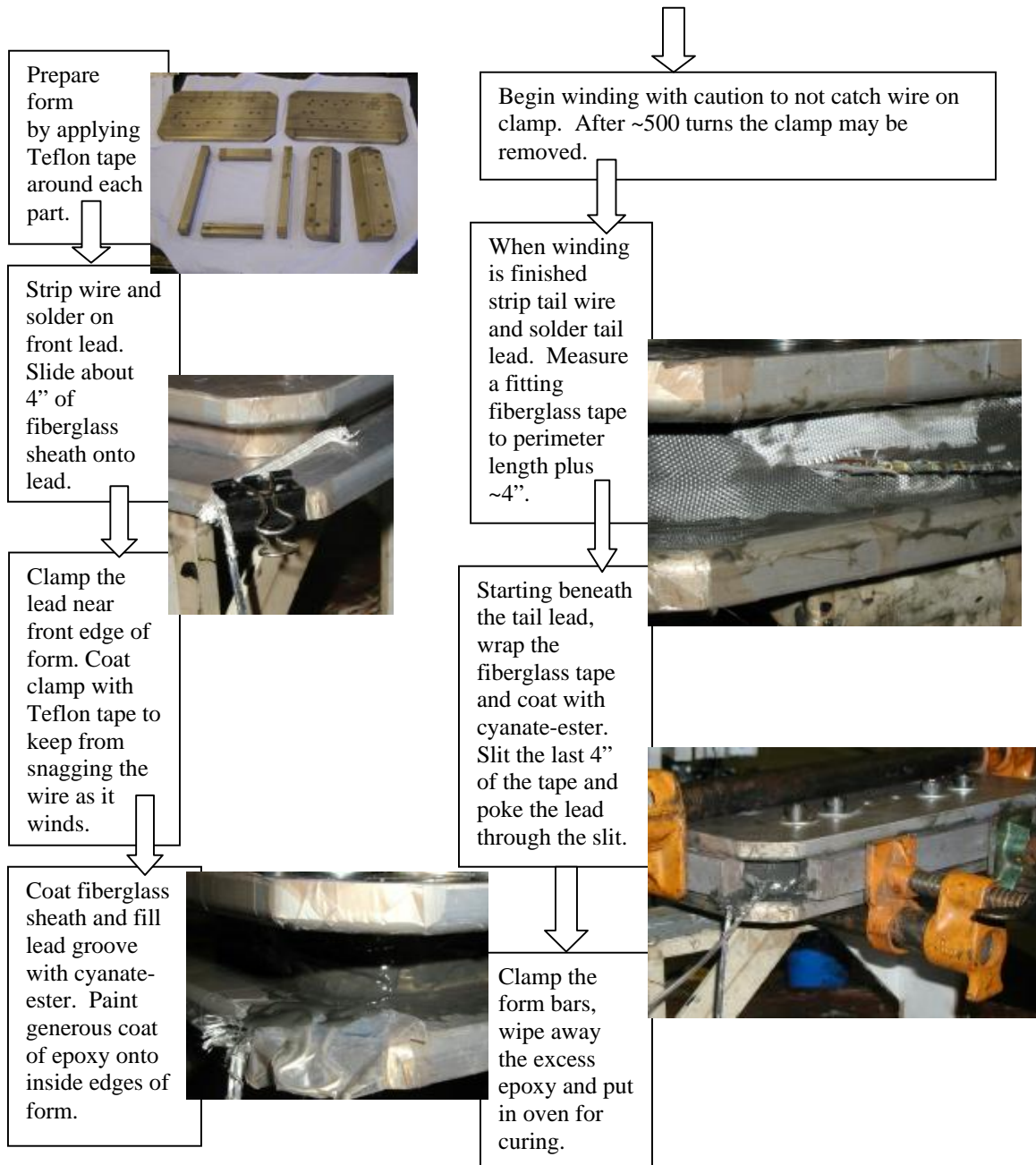
The first step to wind the cyanate-ester coils was to cover the aluminum winding form (the mold that the wire wraps around to give the coil the correct shape) with Teflon® tape. The form was then held together using steel bolts into threaded holes in the bottom plate of the form. Next, the coil-winding machine was setup by assembling the parts, setting the desired wire tension, and bolting the complete form onto the coil-winder. The end of the wire was pulled out from the wire spool, stripped of insulation, and soldered to a thicker wire called the front current lead. A four-inch long piece of fiberglass woven sheath (about .5" diameter) was inserted onto the front lead just past the groove in the magnet form and the lead was clamped there using a Teflon®-tape-coated binder-clip at the edge of the form. A strip of Kapton® was inserted above it to keep the coil wires from cutting through the fiberglass and shorting to the lead.

The cyanate-ester was warmed for about an hour at 40° C, and then it was then mixed up by adding 60 parts of hardener to each 100 parts of cyanate ester resin. Next the cyanate-ester was painted generously onto the fiberglass sheath and around the inside of the form. The winding process was then started slowly and with caution so as not to catch the wire on the clip clamping the front lead. After approximately 500 turns around the form the coil wires served to clamp the lead and so the clip was removed. When the winding completed at 2200 turns the coil wire was stripped and a back lead similar to the front was soldered on. After this, fiberglass tape, matched to the height of the coil, was measured to the inside perimeter plus about four inches. The tape was wrapped around the coil, starting just underneath the back lead. As the tape completed one turn around

the inside perimeter of the coil a slit was made such that the back lead would be able to fit through. The tape was wrapped the rest of the way and painted with the cyanate-ester.

Then form bars were clamped into the form to compress the coil wires. Following this, the coil was put into a pizza oven connected to a computer controlled power source. The cyanate-ester needed a special heating cycle to cure and the computer was set to cycle the oven to the cure cycle: Ramping the temperature to 90 deg. C and soaking for 4 hours then ramping the temperature to 177 deg. C and soaking for 4 hours.

5.2 Cyanate-Ester Winding Photo Flow-Chart



5.3 Gandalf Input File for MOCICC Dipole; Operation in 4 W/m Heating

MOCICC 4W_m heating normal operation

&INDATA

```
NELEMS=      100, XLENGT=      3.6576, ITYMSH=      1,
NELREF=      50, XBREFI=      1.46, XEREFI=      2.2,

ICHFUN=      0,
AHEH  =  0.0, AHEB  =  1.976E-5,
DHH   =  0.0, DHB   =  0.001,
PHTHB =  0.0, PERFOR=      0.0,

ICBFUN=      0,
ISC   =  31, ASC   =  2.77E-6,
E0    =  1.0E-4, NPOWER=      30, EPSLON=-0.99,
IST   =  1, AST   =  5.53E-6, RRR   =  100.0,
IJK   =  13, AJK   =  1.90E-5,
IIN   =  21, AIN   =  2.89E-5,
PHTC  =  0.055, PHTJ =  0.0178, PHTCJ =  0.0107,

INTIAL=      2,
PREINL= 5.0E+5, TEMINL=      4.2, MDTINL=  5.0E-3,

IOPFUN=      0, IOP0  =  1.0E+4,   TAUDET=0.01,
TAUDUM=0.1,

IBIFUN=      0, BISS  =  1.0, BOSS  =  2.0,

IQFUN  =      0,

Q0     =  4, XQBEG =  0.1, XQEND =  3.6,
TAUQ  = 10.0,

TEND  = 10, PSTEP =  1.0, GSTEP =  0.1,

STPMIN=  1.0E-3, STPMAX=  0.1,

METHOD=      0,

ISTORP=      1, IRESTA=      0, MONITR =      1,
```

&END

6 BIBLIOGRAPHY

Ref. 1: Available: http://www.gsi.de/zukunftsprojekt/index_e.html.

Ref. 2: Sherrill, B. S., "Overview of the Rare Isotope Accelerator Project," in *NINB* 204, 2003, pp 765-770.

Ref. 3: A. F. Zeller, V. Blideanu, R. M. Ronningen, B. M. Sherrill, R. Gupta, "Radiation Resistant Magnets for the RIA Fragment Separator," *Particle Accelerator Conference, 2005. PAC 2005. Proceedings of the*, vol., no.pp. 2200- 2202, 16-20 May 2005.

Ref. 4: A. F. Zeller, J. C. DeKamp, and J. DeLauter, "A radiation resistant dipole," *IEEE Transactions on Applied Superconductivity*, vol. 15, no. 2, pp. 1181-1184, June 2005.

Ref. 5: A. F. Zeller, J. C. DeKamp, J. DeLauter, and A. Ghosh, "Metal oxide CICC for radiation resistant magnets," *Advances in Cryogenic Engineering –ICMC*, vol. 52, pp. 575-581, 2006 American Institute of Physics.

Ref. 6: M. Winkler, M. Svedentsov, K.-H. Behr, H. Geissel, H. Iwase, G. Moritz, C. Muhle, H. Weick, "Radiation Resistant Quadrupole Magnet for the Super-FRS at FAIR," *IEEE Transactions on Applied Superconductivity*, vol.16, no.2pp. 415- 418, June 2006.

Ref. 7: R. Reed and D. Evans, "Insulation Systems for Muon Collider," *Report to A. Zeller (unpublished)*, Cryogenic Materials, Inc. April, 2000.

Ref. 8: J. Schultz, "Radiation resistance of fusion magnet materials," *20th IEEE/NPSS Symposium on Fusion Engineering*, pp. 423- 426, 14-17 Oct. 2003.

Ref. 9: A. Harvery and S. A. Walker, "High current density coils for high radiation environments," *IEEE Trans. Nucl. Sci.*, vol. NS-16, pp. 611-613, 1969.

Ref. 10: D. George, "Magnets with mineral-insulated coils at SIN," in *Proc. Of MT-5*, pp. 719-722, 1975.

Ref. 11: American Magnetics, available: <http://www.americanmagnetics.com/>.

Ref. 12: M. Wilson, "Computer simulation of the quenching of a superconducting magnet," RHEL/M 151, unpublished, 1968.

Ref. 13: Poisson Superfish, Los Alamos Accelerator Code Group, Los Alamos National Laboratory.

Ref. 14: A. F. Zeller, R. Zink, J. Wagner, S. Hitchcock, J. C. DeKamp, and A. Balaint, "Testing of large aperture superferric quadrupoles," *IEEE Transactions on Applied Superconductivity*, vol. 9, no. 2, pp. 693-696, June 1993.

Ref. 15: K. Bittner-Rohrhofer, P. Rosenkranz, K. Humer, H. W. Weber, J. A. Rice, P. E. Fabian, and N. A. Munshi, "Characterization of reactor irradiated organic and inorganic hybrid insulation systems for fusion magnets," *Advances in Cryogenic Engineering*, vol. 48A, pp. 261-268, 2002.

Ref. 16: M. Sawan, P. Walstrom, "Superconducting magnet radiation effects in fusion reactors," *Fusion Technology*, vol. 10, p. 741, 1986.

Ref. 17: R. Gupta, M. Anerella, M. Harrison, W. Sampson, J. Schmalzle, R. Ronningen, and A. Zeller, "Radiation resistant HTS quadrupoles for RIA," *IEEE Transactions on Applied Superconductivity*, vol. 15, no. 2, pp. 1148-1151, June 2005.

Ref. 18: Gandalf v.2.2, Cryosoft, 2001.

Ref. 19: J. Baldzuhn, H. Ehmler, A. Hoelting, K. Hertel, C. Sborchia, L. Genini, T. Schild, "Coil tests and superconductor code calculations for the stellarator W7-X coils," *Cryogenics*, vol. 46, issues 7-8, pp. 507-516, July-August 2006.

Ref. 20: A. Zeller, private communication, Nov. 2006.

Ref. 21: A. Harvey, "Experience with the LAMPF Mineral-Insulated Magnets," MT-6, Bratislava 551 (1977).

Ref. 22: S. W. Schwenterly, "Design and testing of electrical insulation for superconducting coils," *Adv. In Cryo. Eng.*, vol 33, pp. 271-281, 1988.

Ref. 23: A. F. Zeller, J. C. Dekamp, "Radiation resistant magnet R&D at the NSCL," *Proceedings of the Particle Accelerator Conference, 2003. PAC 2003.*, vol.1, no.pp. 161- 163 Vol.1, 12-16 May 2003.